European Journal of Applied Sciences – Vol. 11, No. 1
Publication Date: January 25, 2023
DOI: 10.14738/aivp.111.13783.
Meurant, R. C. (2023). Core–Shell and Core–Multi-shell Configurations of the Polyhedra According to the Separation of Faces, and their Interlayer Polytopes. European Journal of Applied Sciences, 11(1). 94–120.

Core–Shell and Core–Multi-shell Configurations of the Polyhedra According to the Separation of Faces, & their Interlayer Polytopes

Robert C. Meurant
Director Emeritus, Institute of Traditional Studies;
Adjunct Professor, Seoul National University PG College of Eng.;
Exec. Director, Research & Education, Harrisco Enco
4/1108 Shin-Seung Apt, ShinGok-Dong 685 Bungi,
Uijeongbu-Si, Gyeonggi-Do 11741, Republic of Korea.

ABSTRACT

The 2.5D cubic schema of polyhedra according to the separation of faces and rhombic schema of faces that I have developed is applied to suggest core–shell and core–multi-shell geometries, using Class II of {2,3,4} symmetry as an exemplary case. The morphology of polyhedra by symmetry class and inclusion of a null element *VP* recognize that each of the 8 Primary Polyhedra (*PP*s) of each class consists of facial polytopes (*PT*s) that include 0-dimensional (0-D) vertices (1-gons), and 1-D edges (2-gons), as well as 2-D polygons (n-gons), where only those *PT*s that lie normal to the axes of symmetry are considered principial. Core–shell configurations are developed for pairs of *PP*s that share an edge of the cubic schema, by locating the smaller *PP* within the larger *PP*, where both are concentric, of unit edge length, and share coaxial negative (–ve), neutral (ntrl), and positive (+ve) axes; in Class II, these consist of facial, edge, and verticial axes of the cube, respectively. Restricting the pairings to the shared edges of the cubic schema that is abstracted from the separation of faces reduces the possible cases in each class from 56 to 12, ensuring their compatibility. The interlayer between inner and outer *PP*s is partitioned into radial prismatic (*PRS*), pyramidal (*PYR*), and truncated pyramidal frustum (*TFM*) (i.e., cupola) elements of (0, α | β, or 2) frequency/orientation according to the rhombic schema of faces (Fig. 1), where 0 refers to the *VT*; α | β in the –ve and +ve cases to facial rotation (truncation), α being the facial *PT* of frequency *n* of the polar (*OH* or *CB*), β of the quasi-regular (*CO*), and in the ntrl case, α | β refer to the PL^{+}–PL^{-} orientations of ntrl *EG*s; and 2 refers to the 2*n* double frequency case. Inner vertices project to outer vertices, ntrl edges, or *n*-gons to form 0-*PRS*s, ntrl 2-*PYR*s, or *n*-*PYR*s; inner ntrl edges project to outer ntrl edges or squares to form 2-*PRS*s or 2-*TFM*s; and inner *n*-gons project to outer *n*-gons or 2*n*-gons to form *n*-*PRS*s or *n*-*TFM*s, while 2*n*-gons project to 2*n*-gons to form *n*-*PRS*s. These are all radial, on the main symmetry axes, and together fill the interlayer space. The heights of these elements are derivable from the inradii of the concentric *PP*s, and show constant increase by gender and axis of the cubic schema. Core–multi-shell configurations are developed by abstracting 4 or 3 consecutive sequences of *PP*s from the cubic schema, thus utilising the core *VP* and/or outer *GR*, respectively, and similarly aligning them coaxially and concentrically; each of the 3 or 2 interlayers thus formed being completely filled by the corresponding *PRS*, *PYR*, and *TFM* elements. The geometries developed might apply to nanoarchitecture, and elsewhere.

Key words: separation of faces, structural morphology, order of polyhedra, core–shell, core–multi-shell, nanostructure

1. THE RHOMBIC SCHEMA AND THE SEPARATION OF FACES IN THE CUBIC SCHEMA

Further inspired by the work of Critchlow [1], and Grünbaum & Shephard [2], and following my much earlier research [3], the rhombic schema that I have earlier developed [4] shows the progression that faces undergo as the steps of the cubic schema progress from VP to GP (Fig. 1). The 0-faces are vertices (VTs); they first progress to α or β faces; −ve & +ve α faces are the (non-verticial) faces of the correspondingly gendered PL, while −ve & +ve β faces are the corresponding faces of the QR, and are rotated (truncated) versions of either α face; ntrl α & β faces are the −ve & +ve ntrl faces (edges) of the −ve & +ve PL, respectively. In Class II, the −ve face is the SQ of the CB, the +ve is the TR of the OH; the ntrl α & β are the edges (EGs) of the OH and CB, respectively. The 2-faces are the double frequency case of the α|β face; in Class II, the −ve, ntrl, & +ve OG, NS, & HX of GR (or of TC, SR, & TO), respectively.

Figure 2 shows the cubic schema that I have earlier developed [4] in horizontal (upper) and bird's eye view (lower) for Class II of {2,3,4} symmetry; it generalizes to all 5 symmetry classes. This schema, which is abstracted from the separation of faces, is critical to exploring the morphology of the polyhedra as they stand in relation to one another, and is central to evincing the various core–shell and core–multi-shell configurations of this paper. Each (gendered) face appears twice in the cubic schema progression; it first appears at spacing of adjoining faces of d=0; then, by the separation of faces, appears at spacing of adjacent faces of d=1. Pairs of the same kind of faces, if adjoining, share a common ntrl VT (NV) or EG (NE); if adjacent, are separated by a NE or ntrl square face (NS). When a PP transforms to another PP in the vertical progression from VP to GP, along the edges of the cubic schema, of the three genders (−ve / ntrl / +ve), the face of one gender undergoes the separation of faces, so those faces remain of the same kind (0, α or β, 2), but the distance apart of adjoining pairs increases by unit (edge) distance to become adjacent pairs. Meanwhile, the faces of the other two genders transform to the next higher state on the rhombic schema. Thus the cubic schema is developed from two rhombic schema (Fig. 1, right), a lower d=0 case of adjoining faces, and an upper d=1 case of adjacent faces. This corresponds to a front horizontal view of the cubic schema.

The cubic schema of two overlaid rhombic schema represents the case for the ntrl faces, presenting the standard horizontal view of the cluster of PPs. Figure 3 shows that rotating the PP cluster by +2π/3 about the vertical $VP-GR$ axis, where individual PPs need also to rotate individually in unison to present the proper face, presents the corresponding schema for the +ve faces; rotating by −2π/3 about the vertical VP–GR axis, it presents the schema for the −ve faces.

Therefore, all cases of concentric aligned inner PP and outer PP are accommodated, as the corresponding inner and outer faces accord with the schema; and thus the interlayer cells described between inner and outer face are either prisms for the separation of faces case, of $VT\rightarrow VT$, α→α or β→β, or 2→2 PRS; or they are transformations of $NV\rightarrow NE$, $VT\rightarrow$α, $VT\rightarrow$β; $NE\rightarrow NS$; or α →2, β →2, which form 2-PYR, α-PYR, β-PYR; 2-TFM; or α-TFM, β-TFM, respectively. Therefore the only kinds of interlayer cells are PRS, PYR, and TFM, in which the 0-PRS is a virtual spike, 2-PYR is an isosceles TR, 2-TFM is a gable, and ntrl α→α and β→β are 2-PRSs, i.e., 2-gon edge prisms (of different orientation). All cells are radially oriented, coaxial to the symmetry axes. This presumes that the inner and outer PP pairs are directly related (share an edge) on the cubic schema. Figure 1 shows these various cases in plan at the mid-points of the edges of the rhombic schema for each gender (left), see also Figs. 3 & 4.

In Fig. 1 below, Ⓐ indicates that Neutral interlayer cells α-*PYR* & β -*PYR* are 2D isosceles *TR*s that span between inner *NV* and outer *NE*, while α-*TFM* & β-*TFM* are gables spanning between *NE* & *NS*; Ⓑ indicates that interlayer cells α & β *PYR* & *TFM* are inserted at mid-points of the rhombic schema between inner and outer faces; meanwhile, *PRS* can be imagined at each node of the generic rhombic schema. Then, Ⓒ indicates that vertical edges show separation of faces, with associated (0, α | β, and 2) *PRS*s; angled edges are corresponding transformations of faces.

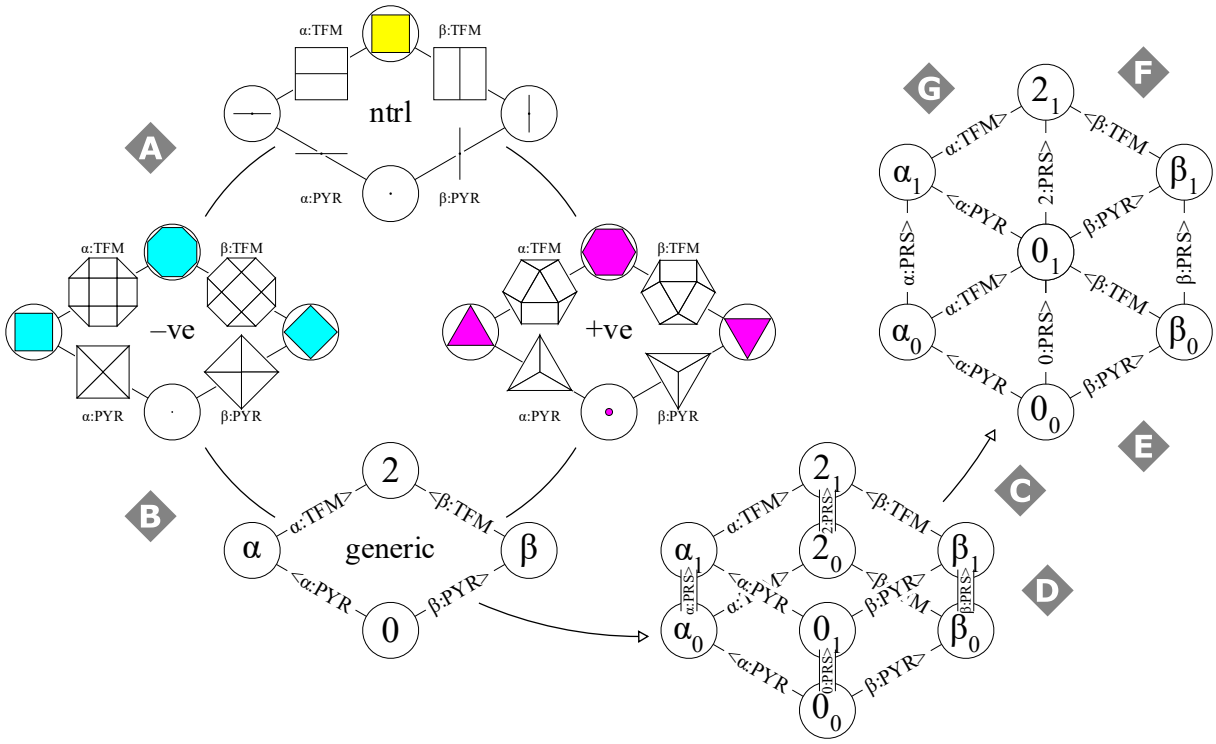

Figure 1: Rhombic Schema of the progression of faces in the cubic schema: Left: Class II −ve, ntrl, and +ve schema of faces; below, generic rhombic schema of faces. Right, development of cubic schema of overlaid rhombic schema; lower rhomb, adjoining faces; upper, adjacent faces; d=0→1.

Next, Ⓓ indicates that the lower rhomb of the two cubic schema at lower and upper right shows the adjoining case of d=0, while the upper rhomb shows the adjacent case of d=1, while Ⓔ indicates that interlayer cells *PRS*, *PYR*, *TFM* start from *VP* with *PRS* or *PYR*, end with *PRS* or *TFM* to *GR*; meanwhile, Ⓕ indicates that angled edges in the schema are associated α|β *PYR*s from 0 faces (*VT*), or α|β *TFM*s to 2 faces (*OG*, *NS*, *HX* by gender). Faces of each gender migrate through the cubic schema from *VP* to *GR* through *PRS*, *PYR*, & *TFM* in various orders. Finally, Ⓖ notes that 2_0 node lies concealed behind 0_1 node at the center of the complex; 2-*PRS* spans between inner 2_0 and outer 2_1 faces.

This analysis assumes and considers principial faces of the *PP*s; a principial face is a polytope (*PT*) of 0D, 1D, or 2D that lies normal to a symmetry axis – so a "face" in my analysis may be a vertex *VT* (1-gon) of 0D, edge *EG* (2-gon) of 1D, or a polygon (n-gon) of 2D. Hence, *VP* is considered to consist of VT^-, VT^0, & VT^+; *OH* of VT^-, EG^0, TR^+; *CB* of SQ^-, EG^0, VT^+; *TO* of RT^-, EG^0, HX^+; *TC* of OG^-, EG^0, RT^+; *SR* of SQ^-, SQ^0, TR^+; and *GR* of OG^-, SQ^0, HX^+ (where $VT^0 = NV$; $EG^0 = NE$; $SQ^0 = NS$). Therefore, *VT*s and *EG*s of the *GR* & *SR*, and *VT*s and some *EG*s (non-*NE*s) of the *TO* & *TC*, are not principial, so are only considered incidentally (as parts of principial *PT*s). This assumption works consistently throughout this analysis and my general exploration [3−14]. A *NV* consists of a 1-gon of 1 *VT* and 1 *EG*, which edge might be considered to be of unit length, coiled up on itself, as in quantum.

Meanwhile, a NE consists of a 2-gon of 2 VTs and 2 colinear EGs. So a NV of the CO can be considered to mediate pairs of adjoining −ve RSs, and of adjoining RTs, while a NV of a VP mediates pairs of adjoining −ve VTs, and of adjoining +ve VTs. While I exploit the limited three-fold symmetry of −ve, ntrl and +ve elements, ntrl elements are fundamentally different from the other two, in being of 2-frequency, with each ntrl element separating two −ve faces on one of its transverse axes, and two +ve faces on the other, orthogonal, transverse axis (PDF 71).

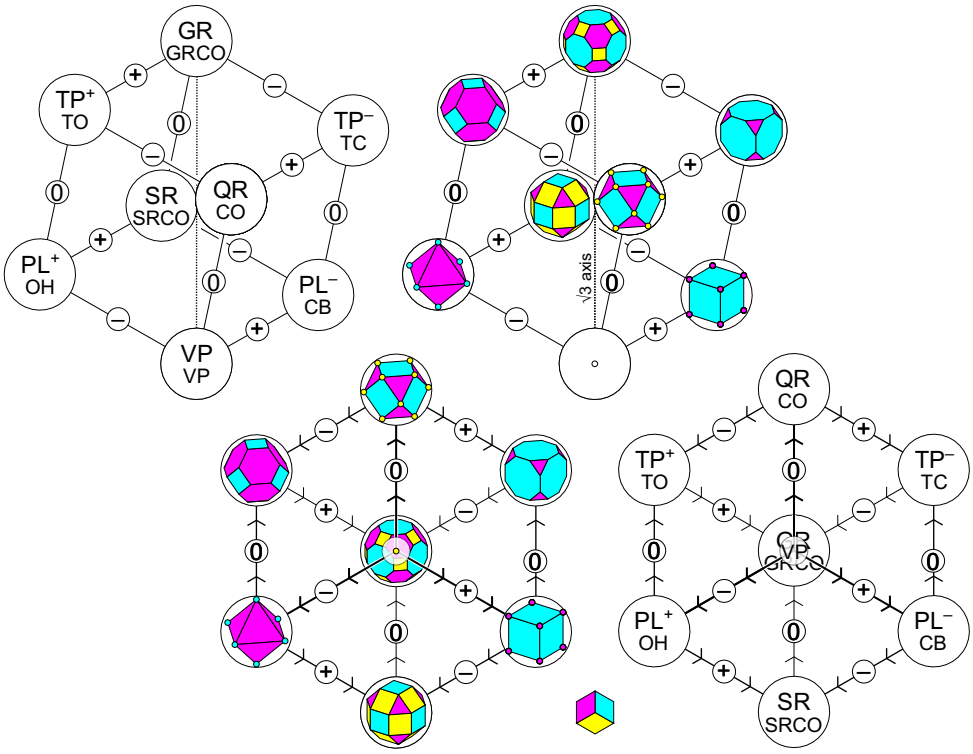

Figure 2: Horizontal views (upper), and views from below (lower), of the cubic schema, showing generic & Class II steps of the separation of faces (outer), and Class II steps of the separation of faces (inner). Horizontal views show separation of −ve faces right to left, ntrl faces below to above, and +ve faces left to right. Views from below show separation by arrows, with VP (closest) and GR (obscured; farthest) at center; out-arrows from source VP, in-arrows toward goal GR (CB shows inverted cubic schema form).

2. CORE–SHELL STRUCTURE IN THE SEPARATION OF FACES

The transitions between PPs generated by the various kinds of separation of faces suggest for the 3D polygonal cases of Classes I–III of {2,3,3}, {2,3,4}, and {2,3,5} symmetry, locating the source PP concentric with the goal PP, and aligning their mutual −ve, ntrl, and +ve axes, to create a core–shell structure, where both core and source PPs are of unit edge length. These configurations might then find applications in diverse fields at varying scale from quantum, nanoscale, human, to large-scale (space structures), and beyond. While the geometry in this section is investigated for the single isolated core–shell case, its applications might be extended to single- or several-layer planar arrays, and to volumetric arrays. It is relevant to note that the 8 PPs of the Class II polygons are also the constituent PPs of Class III of the all-space-filling {2,3,4}|{2,3,4} periodic arrays of the regular and semi-regular polyhedra (the 3D honeycombs), and together with the PPs of Class I of the polyhedra, constitute the PPs of Class II of the all-space-filling {2,3,3}|{2,3,4} periodic arrays (honeycombs), while 4 of the PPs of the Class I polyhedra are the constituents of the singular all-space-filling {2,3,3}|{2,3,3} periodic array.

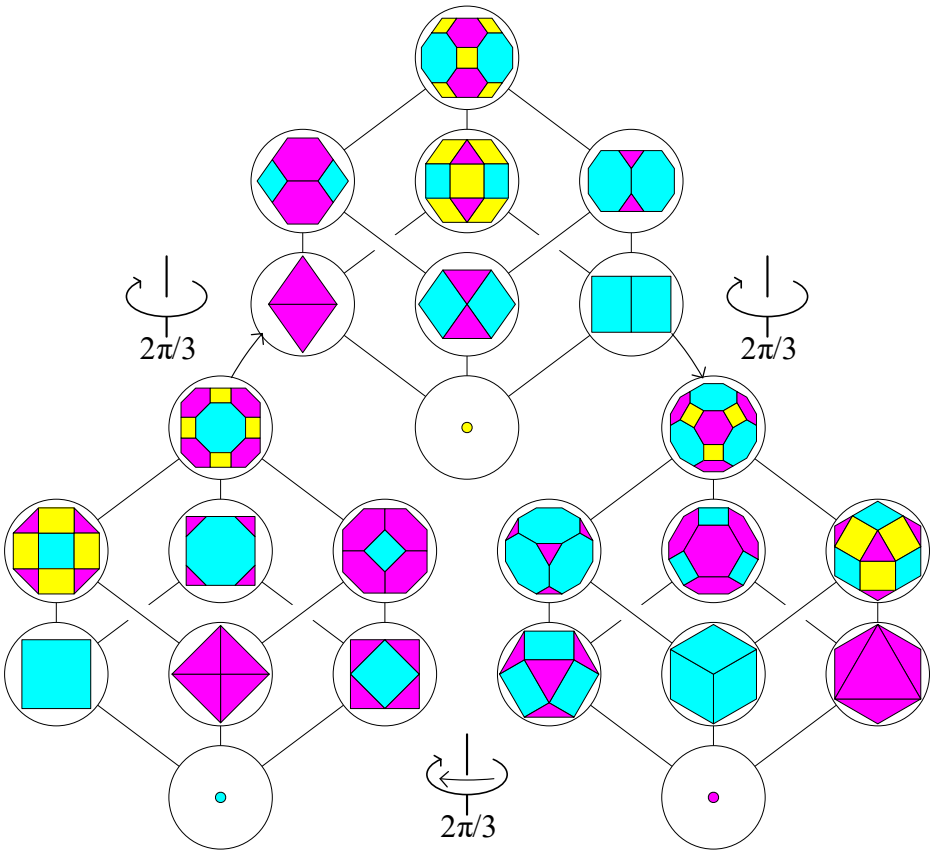

Figure 3: Rotations by 2π/3 of the Class II cubic schema about the schema's vertical $GP-VP$ axis. The rotations provide snapshots that reflect the vertical correspondence of facial separation of d=0 and d=1 (lower to upper). In addition to the $GR-VP$ axial rotation of the PP cluster, to present the appropriate face, each 3D PP also needs to rotate individually, but in parallel, by a common angle: ntrl → +ve, (110)→(111); +ve → −ve, (111)→(000); −ve → ntrl, (000)→(110)). The PP cluster rotates to present different gender of faces of the same or reflected formal structure.

I postulate that the morphology of space that these various configurations delineate underlies the potential form that space can support in terms of quantum phenomena, molecular structure, nanoarchitecture, chemical compounds, crystalline forms, and space structures, unless it is found that space itself can vary at different scale, e.g., at the quantum level and nanoscale. This recognizes that the geometric potential of empirical space as evidenced in these configurations and relationships is not specifically bound in terms of location, scale, or orientation, but does demonstrate some of the very real constraints on what is possible within space, and its inherent capacity to articulate harmonic structure. In later work, I expect to extend these principles to the polygonal arrays of Classes IV & V of the regular and semi-regular polytopes that constitute the all-space-filling {2,3,6} and {2,4,4} periodic arrays of polygons that are the regular and semi-regular tessellations of the plane, replacing the equal edge length by equal period length.

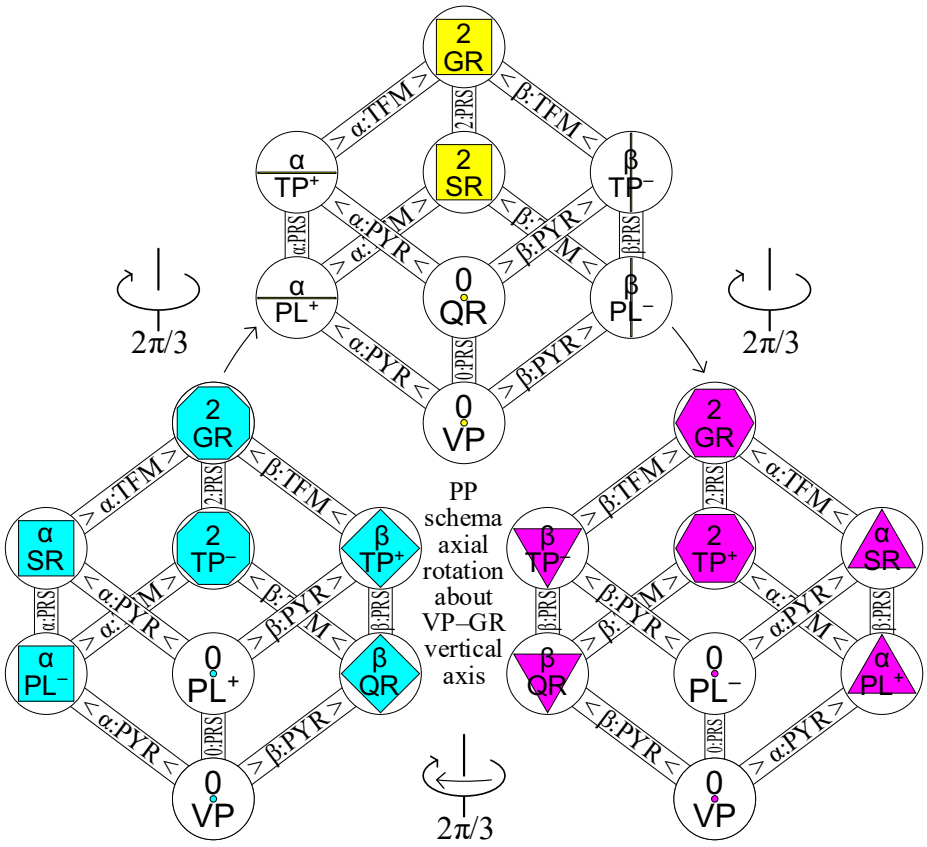

Figure 4: Class II cubic schema of the separating −ve, ntrl, or +ve faces at left, above, and right, respectively; according to the 2π/3 rotations of the cubic schema of PPs about the schema's vertical $GP-VP$ axis. The interlayers of the −ve, ntrl, and +ve schema are composed of (0, α | β, or 2) PRSs, (α or β) PYRs, or (α or β) TFMs, and are derived at each axial rotation of faces. The ntrl α | β schema differs significantly from the −ve & +ve α | β schema, although deeply akin. The same formal/reflected structure is seen in the interlayer cases derived from the pairings of faces.

In the transition from core to shell, of inner PP to outer PP, the 2D polygons of the separating faces generate radial polygonal prisms. (A familiar example is the CB inside $SRCO$, where separating −ve SQ faces of the CB generate SQ prisms that are cuboids of $1 \times 1 \times 1/\sqrt{2}$ size). In any particular case, the separation of faces of one gender is accompanied by the transformation of the faces of the other two genders; in the interlayer between inner and outer PP, these form radial PYRs and TFMs, so that the interlayer space is filled with radial PRSs, PYRs, and TFMs. Allowing ntrl 1D faces of edge (E) to generate edge prisms (E-PRS), and −ve, ntrl, and +ve 0D faces of V to generate vertex prisms (V-PRS), it becomes evident that in each of the 3 classes of regular and semi-regular polyhedra, just 12 such core–shell structures can be found, i.e., 4 for each of the −ve, ntrl, and +ve separation of faces, which underlies the cubic schema. In each class, $Core \rightarrow Shell$: Step 1. $VP \rightarrow PL^+$, $VP \rightarrow QR$, and $VP \rightarrow PL^-$; Step 2. $PL^+ \rightarrow SR$ and $PL^+ \rightarrow TP^+$, $QR \rightarrow TP^+$ and $QR \rightarrow TP^-$, $PL^- \rightarrow TP^-$ and $PL^- \rightarrow SR$; Step 3. $TP^- \rightarrow GR$, $SR \rightarrow GR$, and $TP^+ \rightarrow GR$. For example in Figs. 2–4, in Class II, the separating −ve and +ve faces of the QR CO on their −ve and +ve axes to the TP^+ TO and TP^- TC will form RS and TR PRSs, respectively, bearing in mind that the inner CO and outer TO and TC are of unit edge length.

Table I shows the 12 separating facial PTs for the generic case and their Core and Shell PTs, while Table II shows the generic and Class I–V separating pairs and their Core and Shell PTs.

Table I. The twelve separating facial *PT*s for the Generic meta-class and their Core & Shell polytopes.

Negative			Neutral			Positive		
Separating facial *PT*s	Source Core *PT*	Goal Shell *PT*	Separating facial *PT*s	Source Core *PT*	Goal Shell *PT*	Separating facial *PT*s	Source Core *PT*	Goal Shell *PT*
F_2^-	TP^-	GR	F_2^0	SR	GR	F_2^+	TP^+	GR
F_β^-	QR	TP^+	F_β^0	PL^-	TP^-	F_β^+	QR	TP^-
F_α^-	PL^-	SR	F_α^0	PL^+	TP^+	F_α^+	PL^+	SR
F_0^-	VP	PL^+	F_0^0	VP	QR	F_0^+	VP	PL^-

NB. $F_0^-=V^-$; $F_0^0=V^0$, $F_\alpha^0=E_\alpha^0$, $F_\beta^0=E_\beta^0$, $F_2^0=F^0$; $F_0^+=V^+$. According to this model, as described in my cubic schema [4], facial polytopes can be VTs (1-gons), EGs (2-gons), or PGs, providing that they are on −ve, ntrl, or +ve symmetry axes, though not all facial *PT*s are so located (e.g., VTs and EGs of $SRCO$ & $GRCO$). The (0, α | β, and 2) faces are as given in my rhombic schema (Fig. 1) [4: Fig. 3].

Table II. Separating PP pairs for the Generic meta-class and Classes I−V and their Core and Shell *PT*s.

CLASS	Negative			Neutral			Positive		
	*PT*s Separate	Source Core *PT*	Goal Shell *PT*	*PT*s Separate	Source Core *PT*	Goal Shell *PT*	*PT*s Separate	Source Core *PT*	Goal Shell *PT*
Generic {ntrl,+,−}	F_0^-	VP	PL^+	F_0^0	VP	QR	F_0^+	VP	PL^-
	F_α^-	PL^-	SR	F_α^0	PL^+	TP^+	F_α^+	PL^+	SR
	F_β^-	QR	TP^+	F_β^0	PL^-	TP^-	F_β^+	QR	TP^-
	F_2^-	TP^-	GR	F_2^0	SR	GR	F_2^+	TP^+	GR
V {2,4,4}	v^-	$vt{:}vt$	$sq{:}vt$	v^0	$vt{:}vt$	$rs{:}rs$	v^+	$vt{:}vt$	$vt{:}sq$
	sq^-	$vt{:}sq$	$sq{:}sq$	e_α^0	$sq{:}vt$	$og{:}rs$	sq^+	$sq{:}vt$	$sq{:}sq$
	rs^-	$rs{:}rs$	$og{:}rs$	e_β^0	$vt{:}sq$	$rs{:}og$	rs^+	$rs{:}rs$	$rs{:}og$
	og^-	$rs{:}og$	$og{:}og$	sq^0	$sq{:}sq$	$og{:}og$	og^+	$og{:}rs$	$og{:}og$
IV {2,3,6}	v^-	$vt{:}vt$	$tr{:}vt$	v^0	$vt{:}vt$	$rt{:}rx$	v^+	$vt{:}vt$	$vt{:}hx$
	hx^-	$vt{:}hx$	$tr{:}hx$	e_α^0	$tr{:}vt$	$hx{:}rx$	tr^+	$tr{:}vt$	$tr{:}hx$
	rx^-	$rt{:}rx$	$hx{:}rx$	e_β^0	$vt{:}hx$	$rt{:}dd$	rt^+	$rt{:}rx$	$rt{:}dd$
	dd^-	$rt{:}dd$	$hx{:}dd$	sq^0	$tr{:}hx$	$hx{:}dd$	hx^+	$hx{:}rx$	$hx{:}dd$
III {2,3,5}	V^-	VP	IC	V^0	VP	ID	V^+	VP	DC
	PN	DC	$SRID$	E_α^0	IC	TI	TR	IC	$SRID$
	RP	ID	TI	E_β^0	DC	TD	RT	ID	TD
	DG	TD	$GRID$	SQ^0	$SRID$	$GRID$	HX	TI	$GRID$
II {2,3,4}	V^-	VP	OH	V^0	VP	CO	V^+	VP	CB
	SQ	CB	$SRCO$	E_α^0	OH	TO	TR	OH	$SRCO$
	RS	CO	TO	E_β^0	CB	TC	RT	CO	TC
	OG	TC	$GRCO$	SQ^0	$SRCO$	$GRCO$	HX	TO	$GRCO$
I {2,3,3}	V^-	VP	TH^+	V^0	VP	OH^*	V^+	VP	TH^-
	TR^-	TH^-	CO^*	E_α^0	TH^+	TT^+	TR^+	TH^+	CO^*
	RT^-	OH^*	TT^+	E_β^0	TH^-	TT^-	RT^+	OH^*	TT^-
	HX^-	TT^-	TO^*	SQ^0	CO^*	TO^*	HX^+	TT^+	TO^*

NB: * denotes colored; OH^* = Tetra-tetrahedron ($TR{:}TR$) (QR); $CO^* = SR\,TR{:}TR$; $TO^* = GR\,TR{:}TR$ [3: Fig. 7]. Refer Nomenclature, p.21; see also my earlier papers.

3. CORE–MULTI-SHELL STRUCTURE

The developed 2.5D schema of the PPs of each class of the polyhedra according to the sequential separation of faces [4] reveals that within each class, 6 core–multi-shell configurations can be advanced, each with core VP (corresponding to its class) and 3 shells, in each case with the outermost shell being the GR QR of that class. These could be differentiated into 2-step sequence (core + 2 layers) from VP, 2-step sequence to GR, as well as 3-step $VP-GR$ (core + 3 layers). Each of the 6 core–multi-shell configurations is characterized by three consecutive steps of separation of −ve, ntrl, or +ve faces, so that the separation of each gender (−ve, ntrl, +ve) can occur only once. Any PP is characterized by a unique combination of realized separations, though the order in which the gendered separation occurs can vary. While the VP is characterized by no separation, PL^+, QR, & PL^- evolve from a single −ve, ntrl, or +ve separation, respectively; TP^-, SR, & TP^+ evolve from two −ve, ntrl, or +ve separations, in either of two ways; and GR evolves from all three −ve, ntrl, and +ve separations in any of 6 different ways. Therefore the 8 PPs show a natural classification into 4 classes of [VP]; [PL^+, QR, & PL^-]; [TP^-, SR, & TP^+]; and [GR], according to their history of facial separation. They also show natural affinities, according to whether they are sequentially related (by the separation of faces/cubic schema). Note also from Table III, center, that the division of the PPs into lower and upper rhombs accords with whether the separation of neutral faces has occurred (d=1), or has not (d=0) (Fig. 1, right). The lower rhomb of <VP, $PL^+|PL^-$, SR> is characterized by the separation of neutral faces not having occurred (d=0), while the upper rhomb of <QR, $TP^+|TP^-$, GR> is characterized by the separation of neutral faces having occurred (d=1); this differentiation accords with a further natural classification of the PPs.

Table III: Constituent PPs of each class as generic expressions of facial separation gender [−|0|+].

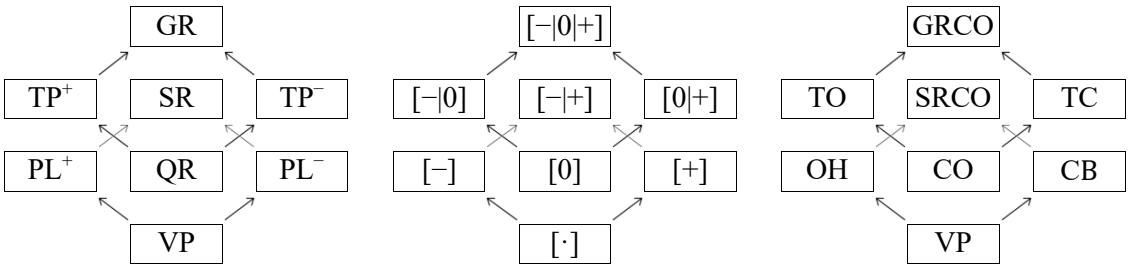

Although there are 8×7 = 56 combinations of regularly situating a PT within another PT of its class, both with unit length, applying the cubic schema organized according to the key separation of faces evolved from the rhombic schema of faces reduces the core–shell combinations to just 12 configurations, whilst guaranteeing the consistency of harmonic cellular partition of the interlayer into radial PRS, PYR, and TFM spatial elements.

Referring to the cubic schema shows that the 12 configurations of paired inner & outer PTs give rise to just 12 2-step configurations of PT in PT in PT, i.e., $VP \rightarrow PT_1 \rightarrow PT_2$, or $PT_1 \rightarrow PT_2 \rightarrow GR$, discounting the skipping of an intermediate PT in the progression from VP to GR. Figure 5 shows the 6 possible 3-step complete sequences that include the source VP and the goal GR; each strand forms a triangular helix on the zonahedral cubic schema, and as observed, comprises a −ve, ntrl, & +ve separation of faces, according to axis, each strand in different overall order. Figures 6 & 7 show the Class II $VP \rightarrow CB \rightarrow SR\ CO \rightarrow GR\ CO$ sequence.

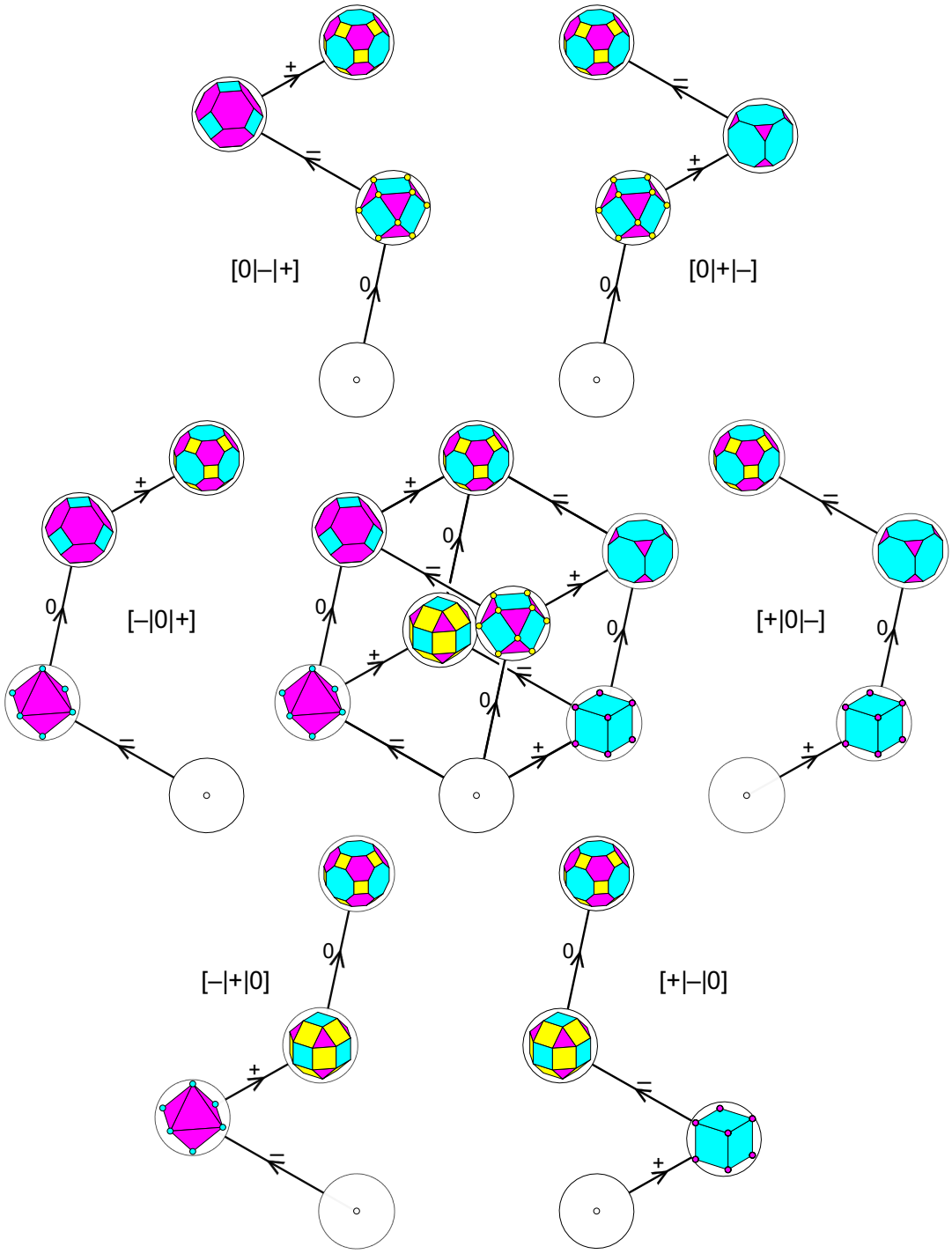

Figure 5: The six multi-shell expansion strands, i.e., triangular helices (core–shell 1–shell 2–outer shell) of Class II in concert, and extracted. Each strand is characterized by 1× −ve, 1× ntrl, & 1× +ve separation of faces, in varied order. Clockwise from 1 o'clock: [0|+|−], [+|0|−], [+|−|0], [−|+|0], [−|0|+], [0|−|+]; views of schema from below of Figs. 14 & 15 show these helices. Core–multi-shell configurations are then formed by arranging the four PTs of each strand concentrically and co-axially (as in Figs. 6 & 7), and except *VP* are of unit edge length. Classes I & III of {2,3,3} & {2,3,5} form similar configurations.

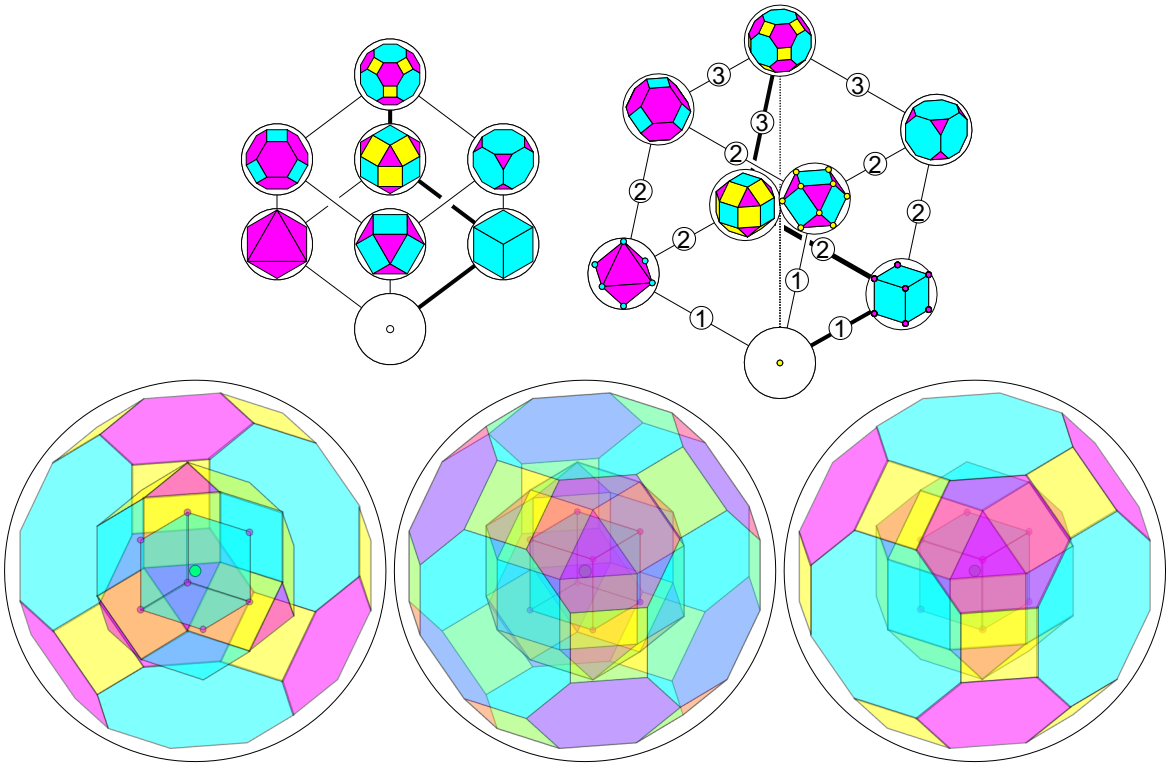

Figure 6: The Class II $VP \rightarrow CB \rightarrow SR\ CO \rightarrow GR\ CO$ sequence, with [+|−|0] order of separation of faces, and unit edge length. Above: 2.5D schema and rotated schema emphasizing the $VP{:}\,CB{:}\,SRCO{:}\,GRCO$ strand. Below: left, interior background multi-shell; center, multi-shell; right: foreground multi-shell.

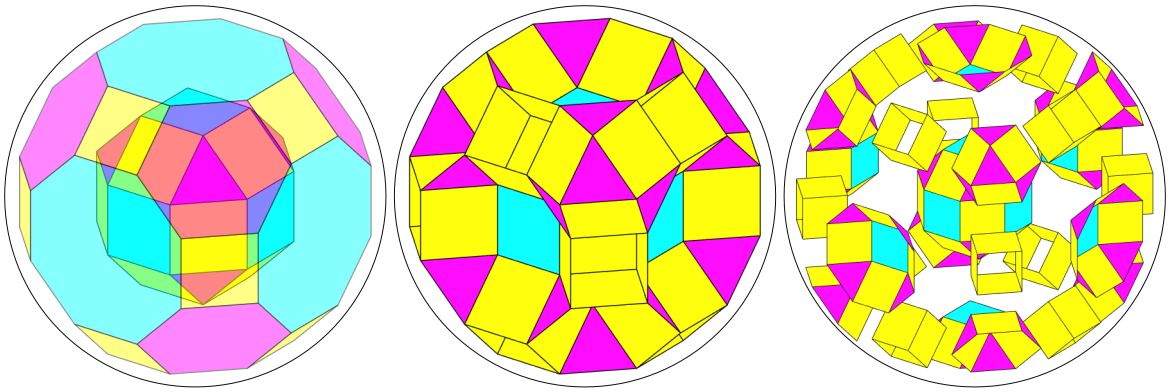

Figure 7: Class II $VP \rightarrow CB \rightarrow SR\ CO \rightarrow GR\ CO$ sequence Left: SR in GR; center, development of interlayer web between SR and GR layers, with TFM_4, TFM_3, and SQ PRSs; right, exploded view.

A convenient example is the Class II $VP \rightarrow CB \rightarrow SR\ CO \rightarrow GR\ CO$ sequence, characterized as the [+|−|0] order of separation of faces, in Fig. 5 lower right, and Fig. 6 top right. In Step 1 of $VP \rightarrow CB$, V^+ separates, while $V^- \rightarrow SQ^-$ and $V^0 \rightarrow E^0_\alpha$. In Step 2 of $CB \rightarrow SR\ CO$, SQ^- separates, while $E^0_\alpha \rightarrow NS$ and $V^+ \rightarrow TR^+_\alpha$. In Step 3 of $SR\ CO \rightarrow GR\ CO$, NS separates, while $SQ^- \rightarrow OG^-$ and $TR^+ \rightarrow HX^+{=}2fTR^+$. So in Step 1 of $VP \rightarrow CB$, the 8 contracted V^+s separate from coincident to cubic array, forming radials of the CB, as the 6 V^-s transform to the 6 SQ pyramids of the cube (of height 1/2); meanwhile, the 12 V^0s extend to E^0_αs. In Step 2 of $CB \rightarrow SR\ CO$, as the 6 contracted SQ^-s separate to form SQ prisms of height √2/2, the 8 V^+s transform to TR pyramids of height √6/6; while the 12 E^0_αs extrude to NSs.

These form the right gables of half CBs cut on the √2 axis of height 1/2. Finally, in Step 3 of $SR\ CO \rightarrow GR\ CO$, as the 12 NSs separate to form NS prisms, the 6 expanded SQ^-s transform to expanded OG^-s, forming a $2SP_8^-$ prism with alternating rectangular and isosceles triangular faces between outer base OG and inner top SQ, while the 8 expanded TR^+s transform to expanded HXs, forming $2SP_6^+$ between outer HX and inner TR. This can be tabulated $VP{:}\,CB{:}\,SRCO{:}\,GRCO$, as below:

Table IV: Class II Core–Multi-shell structure by shell sequence, step, gendered inner and outer face, and gendered interlayer all-space-filling prism, pyramid, and truncated pyramidal frustum.

Multi-shell	PT shell sequence	Step	Negative			Neutral			Positive		
			Inner *PT* shell	Inter-layer *PT* shell	Outer *PT* shell	Inner *PT* shell	Inter-layer *PT* shell	Outer *PT* shell	Inner *PT* shell	Inter-layer *PT* shell	Outer *PT* shell
$TC{:}\,CO$	$GRCO$ $TC{:}$ $CO{:}$ $VP{:}$	3	OG_0^-	PRS_8^-	OG_1^-	E_1^0	TFM_2^0	SQ_1^0	RT_1^+	TFM_3^+	HX_1^+
		2	RS_0^-	TFM_4^-	OG_0^-	V_1^0	PYR_2^0	E_1^0	RT_0^+	PRS_3^+	RT_1^+
		1	V_0^-	PYR_4^-	RS_0^-	V_0^0	PRS_1^0	V_1^0	V_0^+	PYR_3^+	RT_0^+
$TC{:}$ CB	$GRCO$ $TC{:}$ $CB{:}$ $VP{:}$	3	OG_0^-	PRS_8^-	OG_1^-	E_1^0	TFM_2^0	SQ_1^0	RT_1^+	TFM_3^+	HX_1^+
		2	SQ_0^-	TFM_4^-	OG_0^-	E_0^0	PRS_2^0	E_1^0	V_1^+	PYR_3^+	RT_1^+
		1	V_0^-	PYR_4^-	SQ_0^-	V_0^0	PYR_α^0	E_0^0	V_0^+	PRS_1^+	V_1^+
SR $CO{:}$ CB	$GRCO$ $SRCO{:}$ $CB{:}$ $VP{:}$	3	SQ_1^-	TFM_4^-	OG_1^-	SQ_0^0	PRS_4^0	SQ_1^0	TR_1^+	TFM_3^+	HX_1^+
		2	SQ_0^-	PRS_4^-	SQ_1^-	E_0^0	TFM_2^0	SQ_0^0	V_1^+	PYR_3^+	TR_1^+
		1	V_0^-	PYR_4^-	SQ_0^-	V_0^0	PYR_α^0	E_0^0	V_0^+	PRS_1^+	V_1^+
SR $CO{:}$ OH	$GRCO$ $SRCO{:}$ $OH{:}$ $VP{:}$	3	SQ_1^-	TFM_4^-	OG_1^-	SQ_0^0	PRS_4^0	SQ_1^0	TR_1^+	TFM_3^+	HX_1^+
		2	V_1^-	PYR_4^-	SQ_1^-	E_0^0	TFM_2^0	SQ_0^0	TR_0^+	PRS_3^+	TR_1^+
		1	V_0^-	PRS_1^-	V_1^-	V_0^0	PYR_α^0	E_0^0	V_0^+	PYR_3^+	TR_0^+
$TO{:}$ OH	$GRCO$ $TO{:}$ $OH{:}$ $VP{:}$	3	RS_1^-	TFM_4^-	OG_1^-	E_1^0	TFM_4^0	SQ_1^0	HX_0^+	PRS_6^+	HX_1^+
		2	V_1^-	PYR_4^-	RS_1^-	E_0^0	PRS_2^0	E_1^0	TR_0^+	TFM_3^+	HX_0^+
		1	V_0^-	PRS_1^-	V_1^-	V_0^0	PYR_α^0	E_0^0	V_0^+	PYR_3^+	TR_0^+
$TO{:}$ CO	$GRCO$ $TO{:}$ $CO{:}$ $VP{:}$	3	RS_1^-	TFM_4^-	OG_1^-	E_1^0	TFM_2^0	SQ_1^0	HX_0^+	PRS_6^+	HX_1^+
		2	RS_0^-	PRS_4^-	RS_1^-	V_1^0	PYR_2^0	E_1^0	RT_0^+	TFM_3^+	HX_0^+
		1	V_0^-	PYR_4^-	RS_0^-	V_0^0	PRS_1^0	V_1^0	V_0^+	PYR_3^+	RT_0^+
			Inner	Interlayer	Outer	In *PT*	Interlayer	Outer	In *PT*	Interlayer	Outer

NB: Superscript is gender. Inner/outer *PT* shell subscript is d = 0 or 1; Interlayer *PT* shell subscript is frequency. SQ^0 is neutral square (NS). Ntrl PYR_2^0 is 2*f* pyramid = radial isosceles TR; PRS_2^0 is radial SQ.

Table V: The 6 generic (above) and Class II (below) multi-shell configurations of the polyhedra.

MS-I	$VP{:}\,QR{:}\,TP^+{:}\,GR$	MS-II	$VP{:}\,PL^+{:}\,TP^+{:}\,GR$	MS-III	$VP{:}\,PL^+{:}\,SR{:}\,GR$
MS-IV	$VP{:}\,PL^-{:}\,SR^-{:}\,GR$	MS-V	$VP{:}\,PL^-{:}\,TP^-{:}\,GR$	MS-VI	$VP{:}\,QR{:}\,TP^-{:}\,GR$
MS-I	$VP{:}\,CO{:}\,TO{:}\,GRCO$	MS-II	$VP{:}\,OH{:}\,TO{:}\,GRCO$	MS-III	$VP{:}\,OH{:}\,SRCO{:}\,GRCO$
MS-IV	$VP{:}\,CB{:}\,SRCO{:}\,GRCO$	MS-V	$VP{:}\,CB{:}\,TC{:}\,GRCO$	MS-VI	$VP{:}\,CO{:}\,TC{:}\,GRCO$

Table VI: The six generic multi-shell (MS I−VI) PP configurations according to facial separation.

	0^{-}_{+}	MS−I $qr{\cdot}tp^{+}$	$-^{+}_{0}$	MS−II $pl^{+}{\cdot}tp^{+}$	$-^{0}_{+}$	M−SIII $pl^{+}{\cdot}sr$	$+^{0}_{-}$	MS−IV $pl^{-}{\cdot}sr$	$+^{0}_{-}$	MS−V $pl^{-}{\cdot}tp^{-}$	0^{+}_{-}	MS−VI $qr{\cdot}tp^{-}$
Shell 3		GR		GR		GR		GR		GR		GR
gender	+		+		**0**		**0**		−		−	
Shell 2		TP^{+}		TP^{+}		SR		SR		TP^{-}		TP^{-}
gender	−		**0**		+		−		**0**		+	
Shell 1		QR		PL^{+}		PL^{+}		PL^{-}		PL^{-}		QR
gender	**0**		−		−		+		+		**0**	
Shell 0		VP		VP		VP		VP		VP		VP

The differentiation of the configurations into their cellular components requires three forms of frequency *f*: the prism (PRS_f); pyramid (PYR_f); and truncated pyramidal frustum (TFM_f). The frequency *f* of the PRS and PYR is of the base; but Fig. 8 shows the original pyramid before truncation is of that frequency, so the frequency *f* of the TPF is of the top (inner PT face); this form thus has a base (outer PT face) of 2*f*, and alternating sidewalls of rectangles (RGs) and isosceles triangles, prototypes being half of the CO cut at one equatorial plane with base HX, top TR, and sidewalls of alternating SQs and regular TRs; or alternatively, the form between −ve SQ top of the CB and −ve OG base of the GR CO, with alternating √2/2 rectangular (RG) and TR sidewalls. The PRS is used for the volumetric element of the separation of faces; if it is the VP that is separating, then PRS_1 is a radial spike, like the radials of the CO; if the (neutral) EG is separating, then PRS_2 is a radial SQ. If VT is expanding to EG, then the radial triangle is a PYR_2. In the case of the neutral EG of the CB to NS of the $SRCO$, the gable form that is formed with 90° apex angle is recognized as the 2*f*-TPF_2 between 2-gon top and SQ base, with two √2/2 RG and two isosceles triangular (TR) sidewalls alternating.

Table VII. Gender & length of interlayer web elements by the separation of faces from PP to PP.

	VP	OH	CO	CB	TO	SR	TC	GR	
GR					$\sqrt{3}/_2$	1	$\sqrt{2}/_2$		GR
TC			$\sqrt{3}/_2$	1				−ve	TC
SR		$\sqrt{3}/_2$		$\sqrt{2}/_2$				ntrl	SR
TO		1	$\sqrt{2}/_2$					+ve	TO
CB	$\sqrt{3}/_2$					−ve	ntrl		CB
CO	1				−ve		+ve		CO
OH	$\sqrt{2}/_2$				ntrl	+ve			OH
VP		−ve	ntrl	+ve					VP
	VP	OH	CO	CB	TO	SR	TC	GR	

For unit core–shell pairs: Above left, length of interlayer web elements; top header, inner PP; left header, outer PP. Below right, gender of separation of faces; right header, inner PP, bottom header, outer PP. For each PRS, PYR, & TFM, for unit length inner and outer PPs, the web edges connecting the two PPs are of equal length of √2/2, 1, or √3/2, dependent on the −ve, ntrl, or +ve separation of faces.

Bold arrows show separation of faces, with constant values of increase in in-radii given in double-line boxes, representing the height, so axial edge, of PRS. PP named at right, gendered face F at left; boxed equation is in-radius. PRS spans between same face type on inner & outer PP.

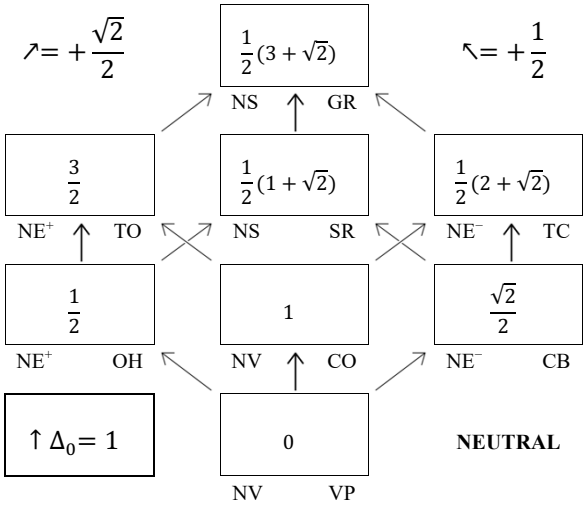

CLASS II INRADII

Light arrows of the other two axes also reveal constant increases, with values given in unboxed equations, represent axial height of the relevant PYR or TFM. PYR spans VT on inner PP to PT on outer PP; TFM spans PT on inner PP to the next PT on the rhombic schema, on the outer PP.

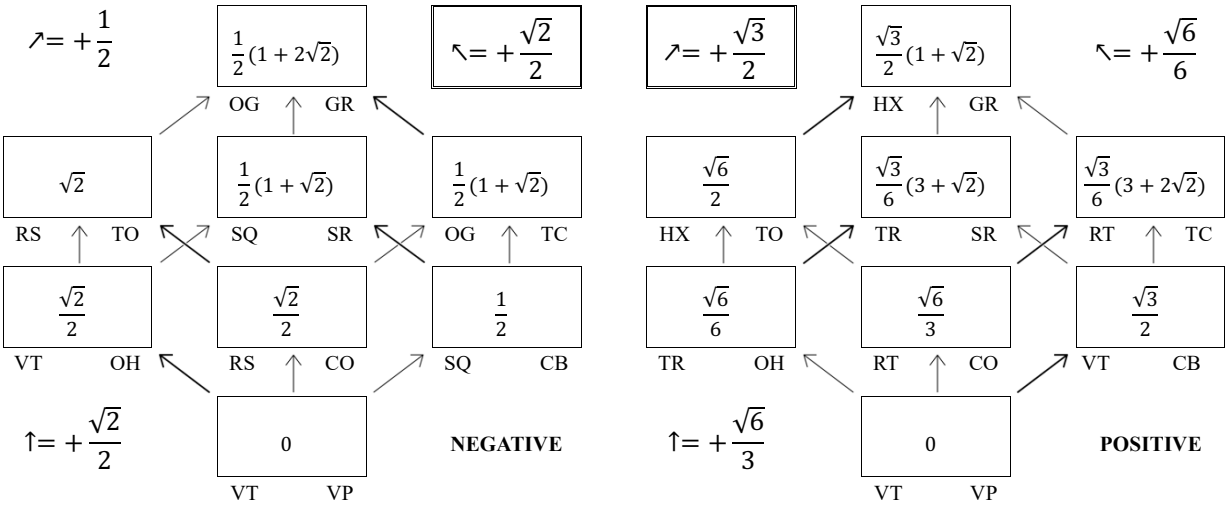

Above: Inradii of PPs for the −ve, ntrl, & +ve separation of faces (bold arrows, double-line boxes).

Circumradii, which do not show constant increase by axis. From the initial progressions from VP to OH, CO, & CB, all other radii can be found by cyclic calculation of circumradius → inradius → different gender inradius → circumradius → different circumradius.

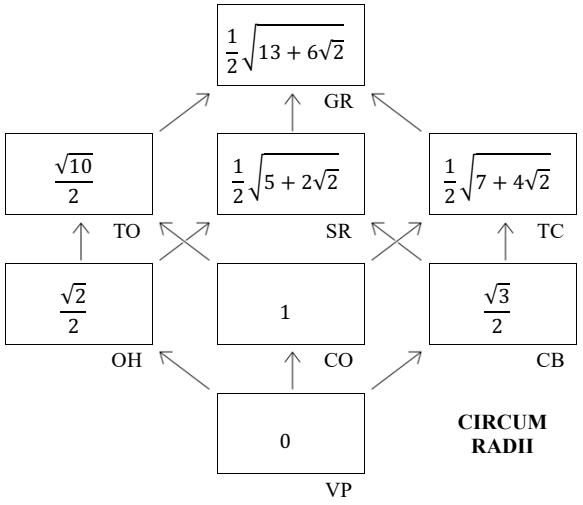

CLASS II CIRCUMRADII

All inradii (above) and circumradii (left) are constructible numbers. The regularity of this order as evident in the constant increases of inradii on each axis further validates the 2.5D cubic schema. Similar relations apply to the other classes of polyhedra, and might be extended to the 2D tessellations.

Figure 8: Radii of the Class II PPs according to the cubic & rhombic schema & separation of faces.

To illustrate the integrity of this system, the $TO - GR$ interlayer, at top left of Fig. 13 (front view of the cubic schema), consists of 4*f* β-TFMs on the −ve axes, 2*f* α-TFMs (gables) on the ntrl axis, and 6*f* 2-PRSs on the +ve (SoF) axis as in Fig. 15 (view of the schema from below); Fig. 8 above shows that these are of height 1/2, √2/2, and √3/2, respectively, all with inclined edge length of √3/2, unit base edge length, and for TFM, unit top edge length. So the various geometries are practical to work with. To clarify, for any given interlayer of the 12 possibilities, the web lengths are equal, and derivable from whether this represents a −ve, ntrl, or +ve SoF; the heights of the three kind of elements in general differ by gender of axis of the interlayer structure, and can be obtained from Fig. 8; and the geometry of the element is thus determined.

The generic configuration of the core–shell structure is thus characterized by just three kinds of polytopes (Fig. 9) that occupy the interlayer spaces between concentric PPs: the (0, α or β, or 2) prism (PRS) generated by the separating set of faces by gender of −ve, ntrl, or +ve; the (α or β) pyramid (PYR) between VT apex and α or β base face; and the (α or β) truncated frustum of pyramid, the Truncated Pyramidal Frustum (TFM; the 'second' truncation occurring after the first truncation of the pyramid to form the frustum, Fig. 10), where the smaller base is the α or β face of the inner PP, the larger base is the 2*f* face of the outer PP, the frequency of the TFM is characterized as the corresponding α or β (the frequency of the original PYR before first or second truncation, which equals the frequency of the TFM top=smaller base), and the side walls of the TFM are alternating isosceles triangles and rectangles. Within the interlayer, the rectangular face of the TFM is also the side face of the corresponding adjacent prism, while the isosceles triangle of the TFM is also the side face of the corresponding adjacent pyramid. Each PRS, PYR, and TFM radiates from the core along a main symmetry axis of the concentric PPs, its main axis being colinear with the symmetry axis. The 0:PRS is a radial edge, a spike from VP=VT to VT, so may be regarded as the prismatic development of the 1-gon VT, PRS_1. The edge prism, PRS_2, is a radial rectangle, as the prismatic development of the 2-gon edge of the d=0 NE of the inner PT to the d=1 NE of the outer PT. The 2-gon pyramid, PYR_2, is an isosceles triangle from apex NV to base NE.

The core–multi-shell configurations are then simply built up by combining sheaths of the different core–shell structures, according to the zonahedral cubic schema and the strands of the triangular helical progressions abstracted in Fig. 5. Each interlayer of the core–multi-shell is accordingly differentiated into PRS, PYR, and TFM elements, and these combine to fill the interlayer space. By proceeding from the cubic schema, the geometry is consistently harmonic, and facile to work with, once the general principles are understood.

Kindly note that my approach is that of an experimental geometer and independent scholar. I have been unable to determine whether these forms have been previously discovered and reported according to any comparable schema, but this work is essentially the result of independent investigation of the polyhedral forms in themselves, whether as isolated forms, familial members, or periodic arrays of the honeycombs; not in what others have reported. This is original and ongoing work, and continually being refined. The combination of the rhombic schema, cubic schema, inclusion of the VP, consideration of principial faces, and recognition of the consistency of behavior across classes of different symmetry provides a highly accessible and imaginable framework for the spatial designer to compose geometric configurations that may be realized as real structure, as well as providing a suitable context for further research.

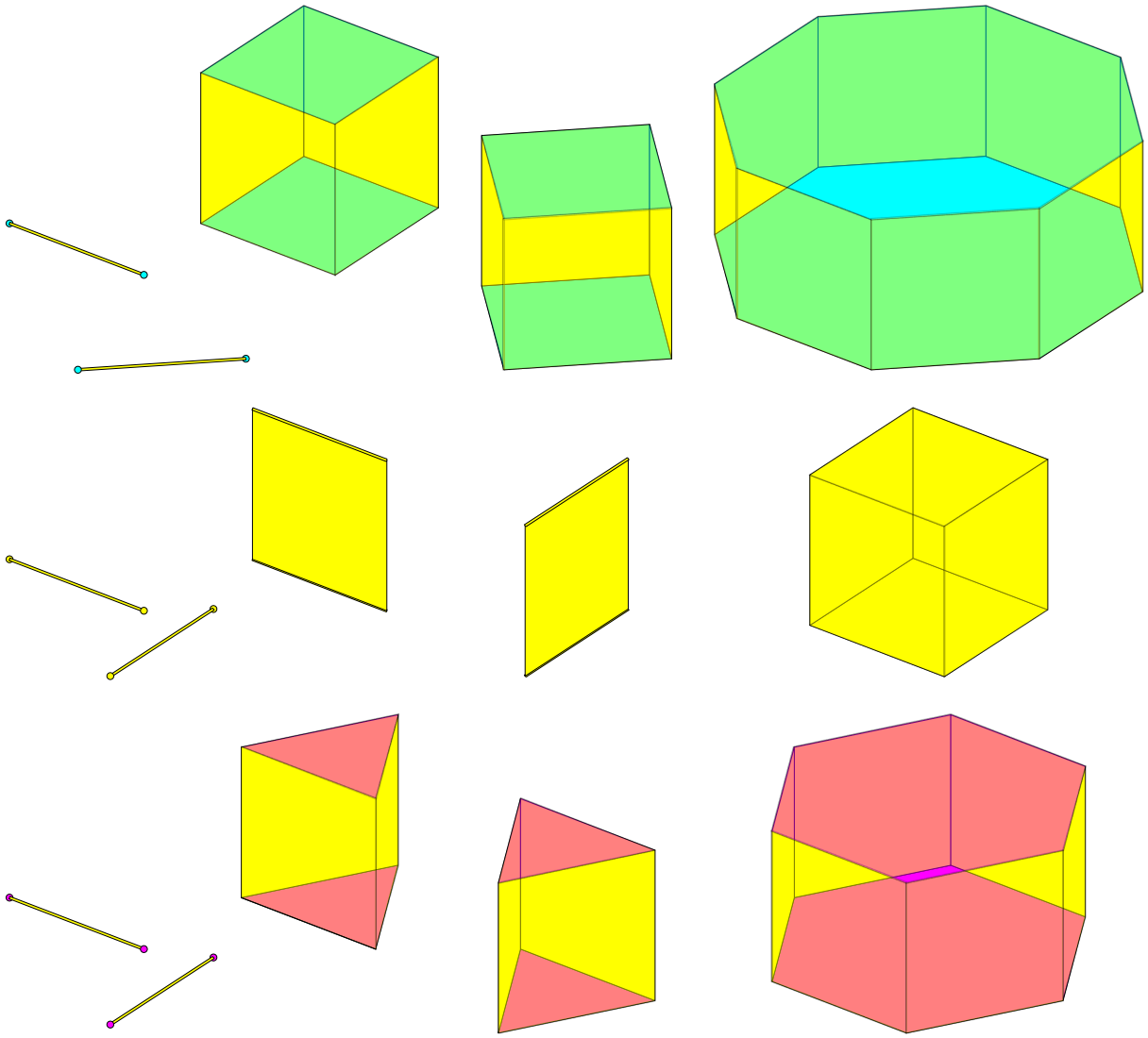

Figure 9A: Class II interlayer web elements for the *neutral* separation of faces, in which all edges are of unit length. Top strata: Negative elements; middle strata: neutral elements; bottom strata: positive elements. Prisms. Columns 1 & 2: 0-dimensional α & β *PRS*s. Cols. 3 & 4: α & β *PRS*s, respectively; neutral is edge *PRS*. Col. 5: 2-frequency *PRS*s.

In the first interlayer from VP to PL^{-}, QR, or PL^{+}, the separating −ve, ntrl, or +ve VTs (only one set per case) form 0-PRS_1s from adjoining d=0 to adjacent d=1 configuration, so form a cluster of virtual spikes from the center (like spicules). Adjacent radials/PRS_1s may also form the pair of equal length edges of the radial 2-gon (flat) PYR_2. Those isosceles triangles also form the faces of the other kind of pyramid.

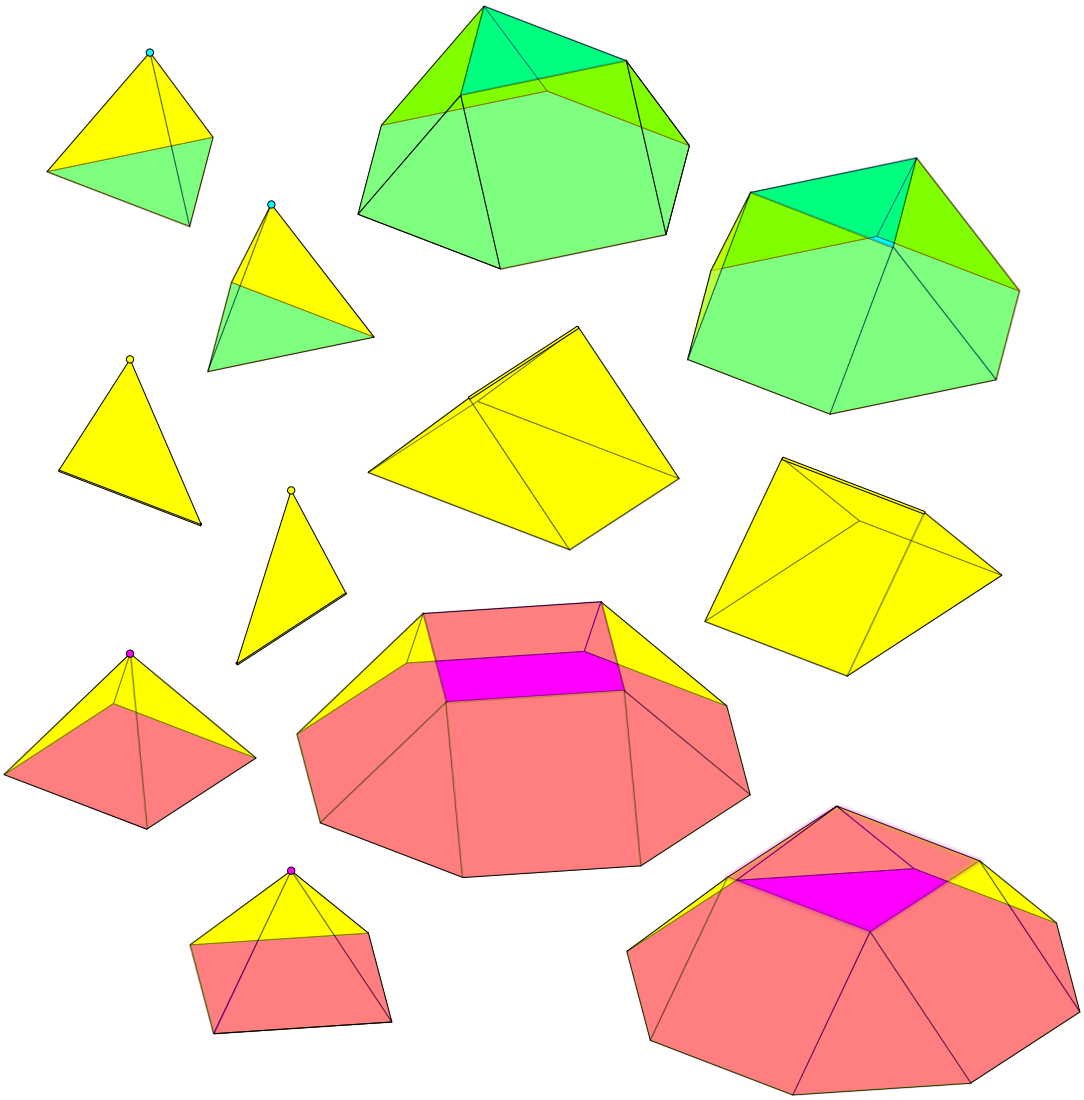

Figure 9B: PYRs and TFMs. Cols. 1 & 2: α & β PYRs, respectively; neutrals are 2-gon edge PYRs. Cols. 3 & 4: α & β TFMs, respectively. Top VT, EG, or PG is of inner PP; Base VT, EG, or PG is of outer PP. Furthermore, the interlayer webs for the −ve, ntrl, and +ve separation of faces each have −ve, ntrl, and +ve elements. For the $-ve$ separation of faces, both the axial edges of PRS and the inclined edges of PYR and TFM are √2/2; for the $+ve$ separation of faces, they are √3/2. In all cases, the base edge lengths, and for the TFMs, the top edge lengths, are of unit length, as facial PTs of the inner or outer PPs characterizing the specific core–shell or shell–shell interlayer.

Adjacent pairs of V_1^0s on the QR form the edges of the base triangles and squares of the component +ve and −ve radial β PYRs, respectively of the interlayer. In the VP–PL^- interlayer, V_0^+s project to form PRS_1 spikes; V_0^-s project to form PYR_4s; and V_0^0s project to form flat isosceles triangular β-PYR_2s. In the VP–PL^+ interlayer, V_0^-s project to form PRS_1 spikes; V_0^+s project to form PYR_3s; and V_0^0s project to form flat isosceles triangular α-PYR_2s. In the three interlayer cases VP–PL^-, $VP-QR$, and VP–PL^+, the +ve, ntrl, and −ve VTs project to PRS_1^+ spikes, PRS_1^0s, and PRS_1^-s, around which 0-PYR^0s and α-PYR^-s, β-PYR^-s and β-PYR^+s, and α-PYR^+s and 0-PYR^0s cluster, respectively.

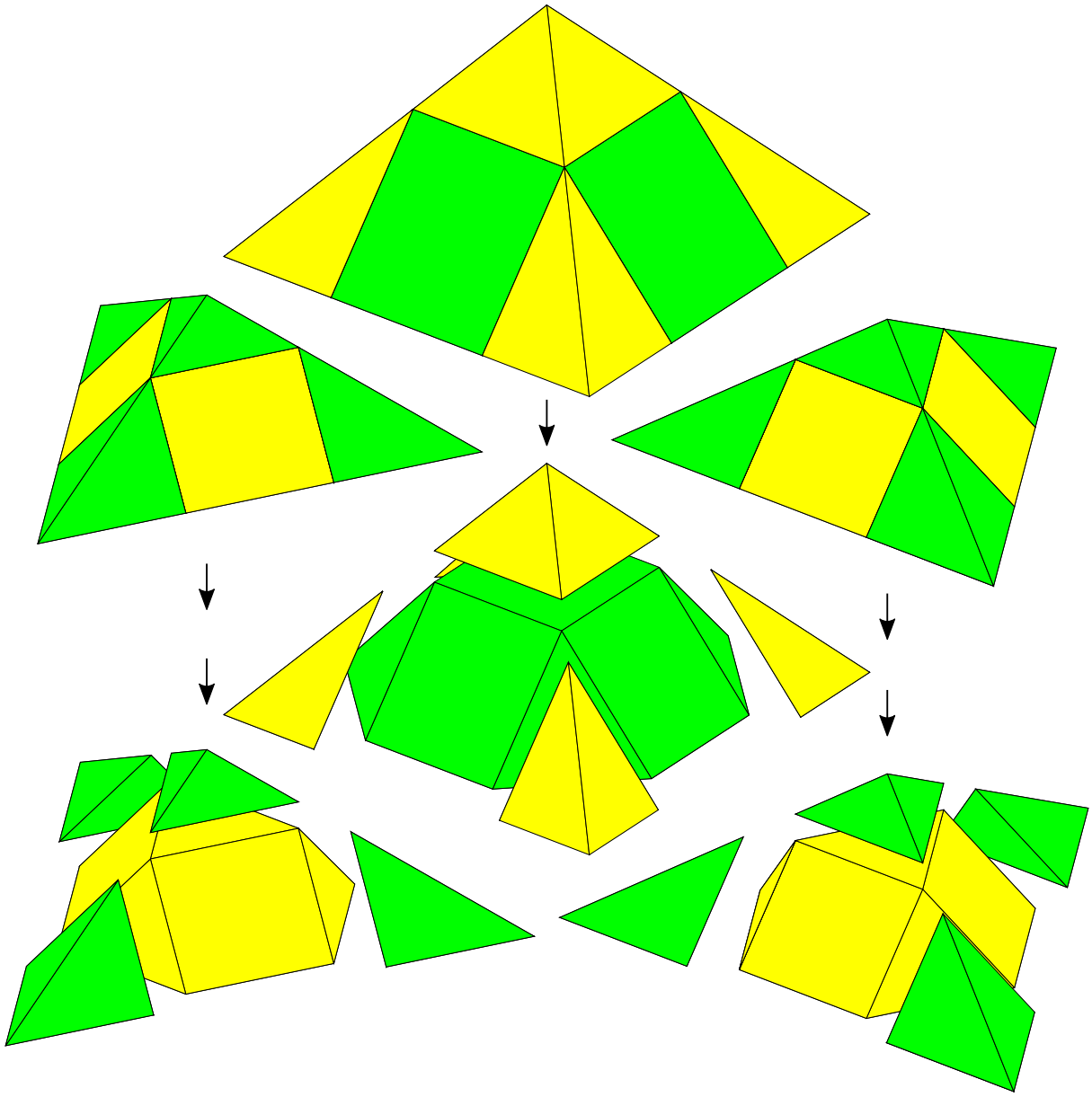

Figure 10. Schematic of the truncations of the parent 3f α- & β-PYR to gain 3f α- & β-TFM, and 4f α-PYR to gain 4f α-TFM: TR: HX for left, α; right, β TR upper base, and center, SQ: OG for SQ upper base. A similar process applies for Class II ntrl 2f, +ve 3f, and −ve 4f faces; also in Class I & III. In all cases, TFM sidewalls alternate rectangles (RG) and isosceles triangular (TR) faces between inner α|β and outer 2α|2β faces of the rhombic schema (vertical dimension indicative only).

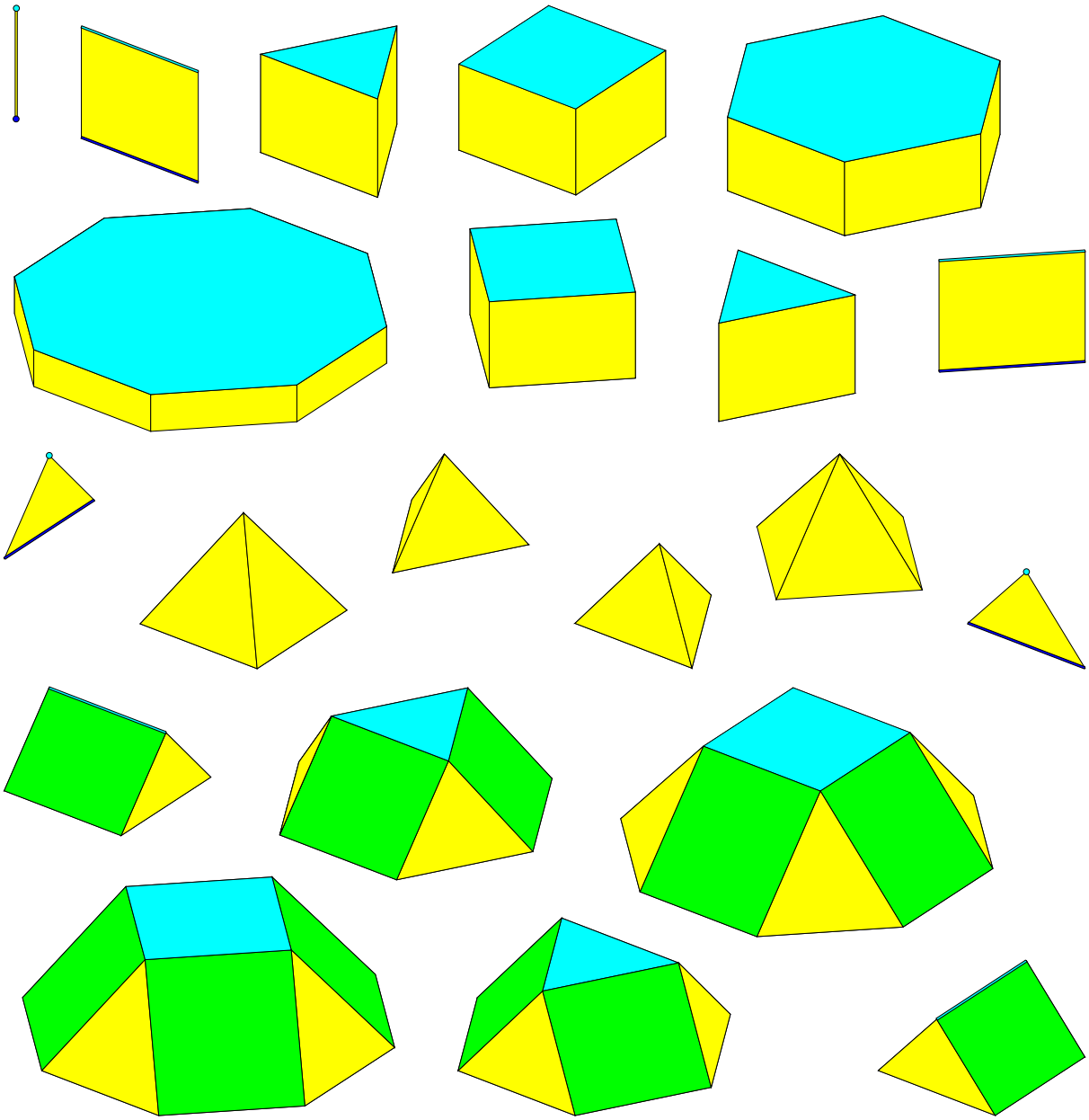

Figure 11. Class II library. Top, Prisms (PRSs): Upper, PRS_1^0, PRS_2^α, PRS_3^α, PRS_4^α, PRS_6^2; lower: PRS_8^2; PRS_4^β, PRS_3^β, PRS_2^β. Middle, Pyramids (PYRs): Upper, PYR_2^α, PYR_3^α, PYR_4^α; Lower, PYR_4^β, PYR_3^β, PYR_2^β. Bottom, Truncated Pyramidal Frusta (TFMs; cupola): Upper, TFM_2^α, TFM_3^α, TFM_4^α; lower: TFM_8^2; TFM_4^β, TFM_3^β. Top (cyan) is of inner PT; outer base of $PRS_2^{\alpha|\beta}$ & $PYR_2^{\alpha|\beta}$ is shown as dark blue. Vertical dimension indicative only; height of element varies by schema axis, as in Fig. 8.

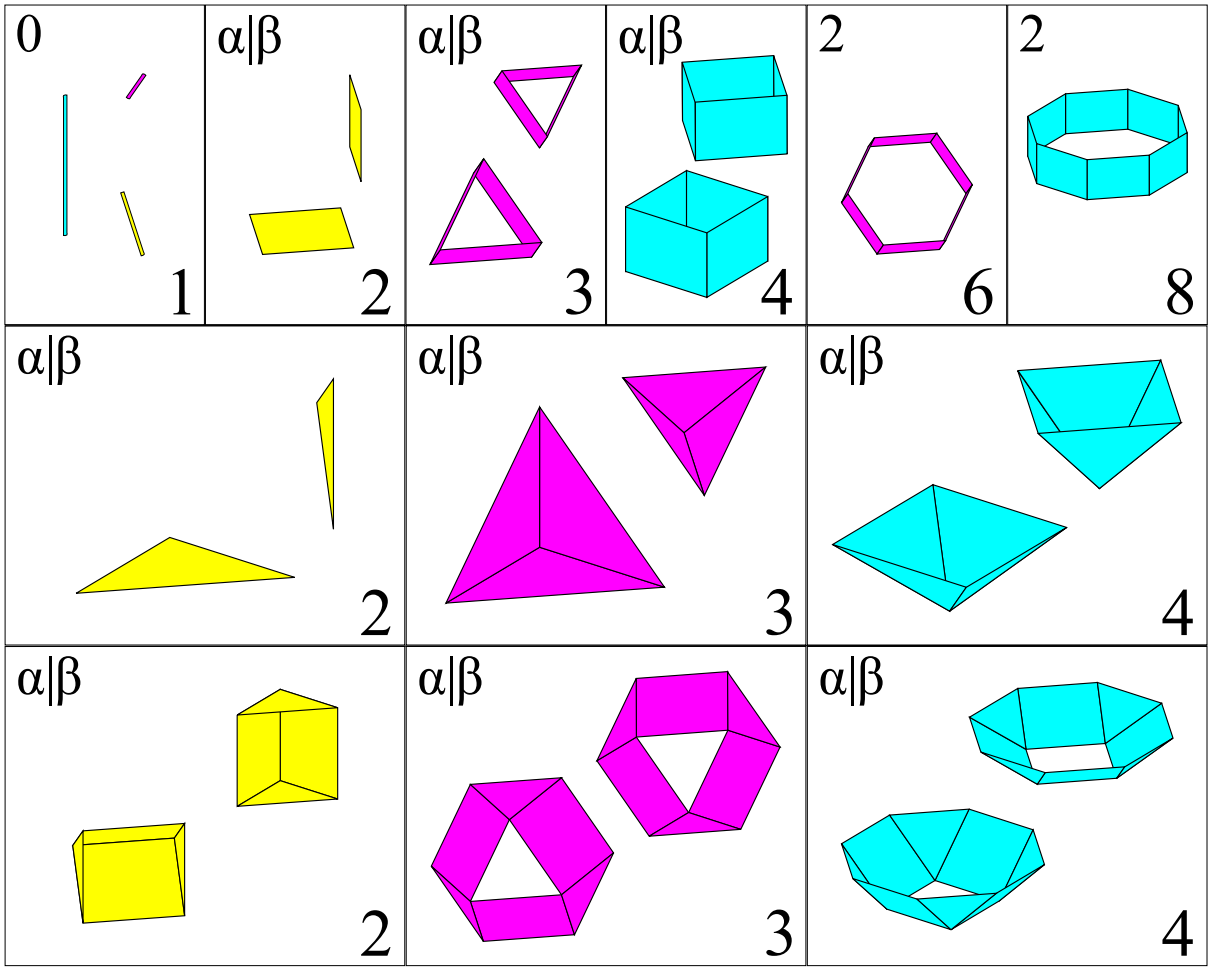

Figure 12: Class II PRS, PYR, and TFM interlayer components. Top, PRS; middle, PYR; bottom, TFM. PRS_1 represents $VP{:}VP$; PRS_2 is $EG{:}EG$ (d=0 to 1). PYR apex is inner facial VT; base is face of outer shell; PYR_2 is $NV{:}NE$. TFM small base is face of inner shell, large base is of outer shell; TFM_2 (gable) is ntrl $NE{:}NS$. Upper left text indicates whether characteristic base is 0, α|β, or 2 frequency face, by the author's rhombic schema of faces (Fig. 1) [4]; lower right shows frequency = symmetry, where $TFM\,f$ is top base = face of inner shell (Figs. 13 & 14). Cyan, –ve; yellow, ntrl; magenta, +ve.

Figure 13 shows the front horizontal view of the cubic schema, situating the large 12 core–shell configurations at the mid-edges between the corresponding pair of small inner and outer PPs. The bilateral symmetry of complements becomes apparent about the vertical axis of the figure, e.g., of +ve/−ve & −ve/+ve PYR; +ve/−ve & −ve/+ve PRS; +ve/−ve & −ve/+ve α- or β-TFM; and ntrl 2-PYR (TR), 2-PRS, 2-TFM; as well as the d=0 to d=1 separations on 3 axes of cells.

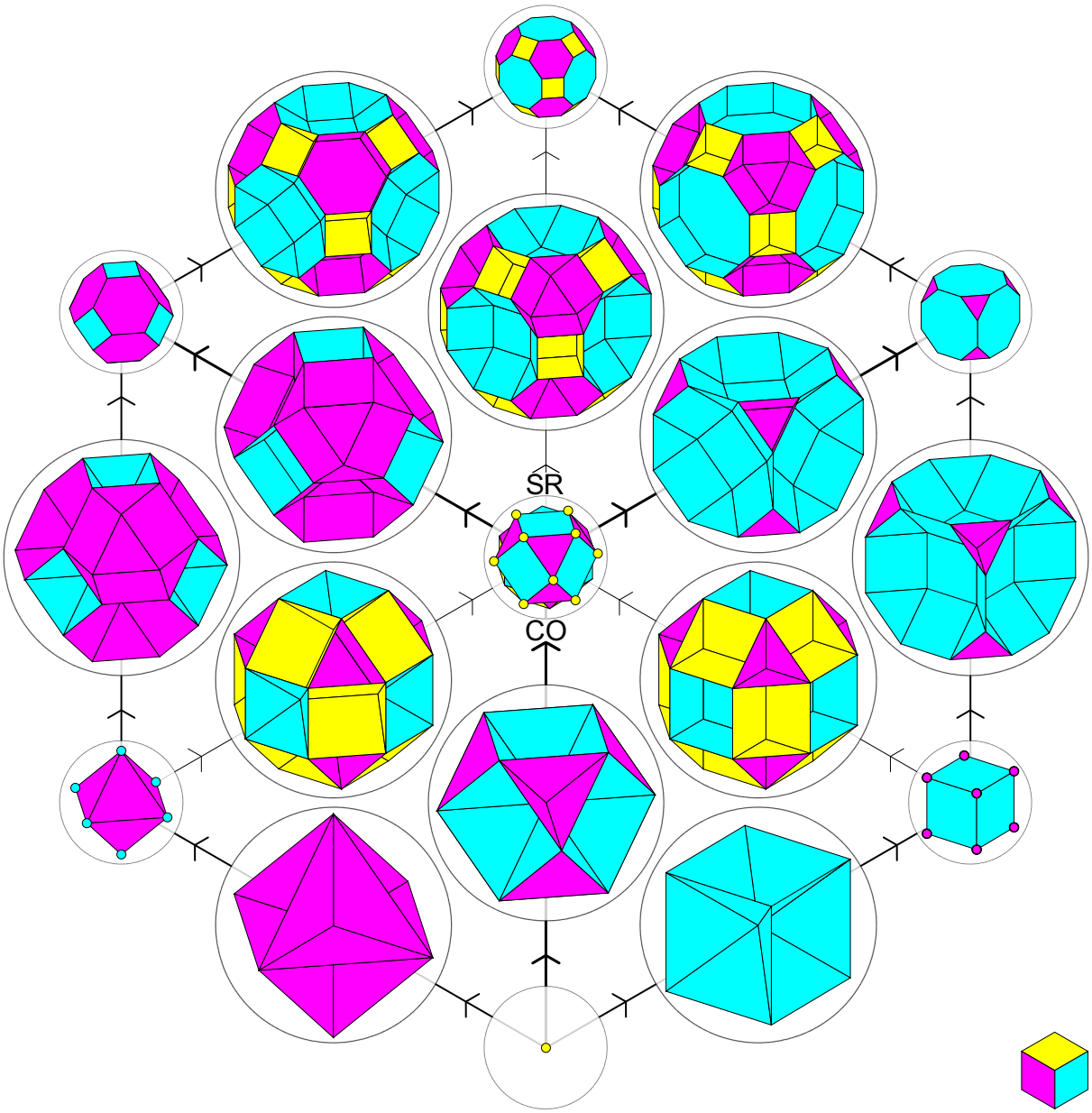

Figure 13A: Class II horizontal 'front' view 2.5D schema of interlayer components between inner and outer PPs, with CO (nearest) and SR (furthest, obscured) at center; GR at top of figure, VP at bottom. Note the bilateral 'symmetry' of complements about the vertical axis $GR-VP$ of ntrl elements of two kinds or orientation, in this paper where the neutral elements are denoted α|β, α being the case for the OH/TO, β for the CB/TC (while for the −ve & +ve elements, α is given by the case for the OH/CB, while β is given by the case for the CO). Also, the complementary PRS & PYR and *vice versa* (bottom rhomb); PYR & TFM horizontal and $PYR:PYR$ & $TFM:TFM$ vertical (middle rhomb); and PRS & TFM and *vice versa* (top rhomb); hence the subtlety of the 2.5D schema that can visualize from the horizontal 'front' the 2-fold, and in Fig. 14, the view from below of 3-fold complementary symmetry, as well as 3D morphology.

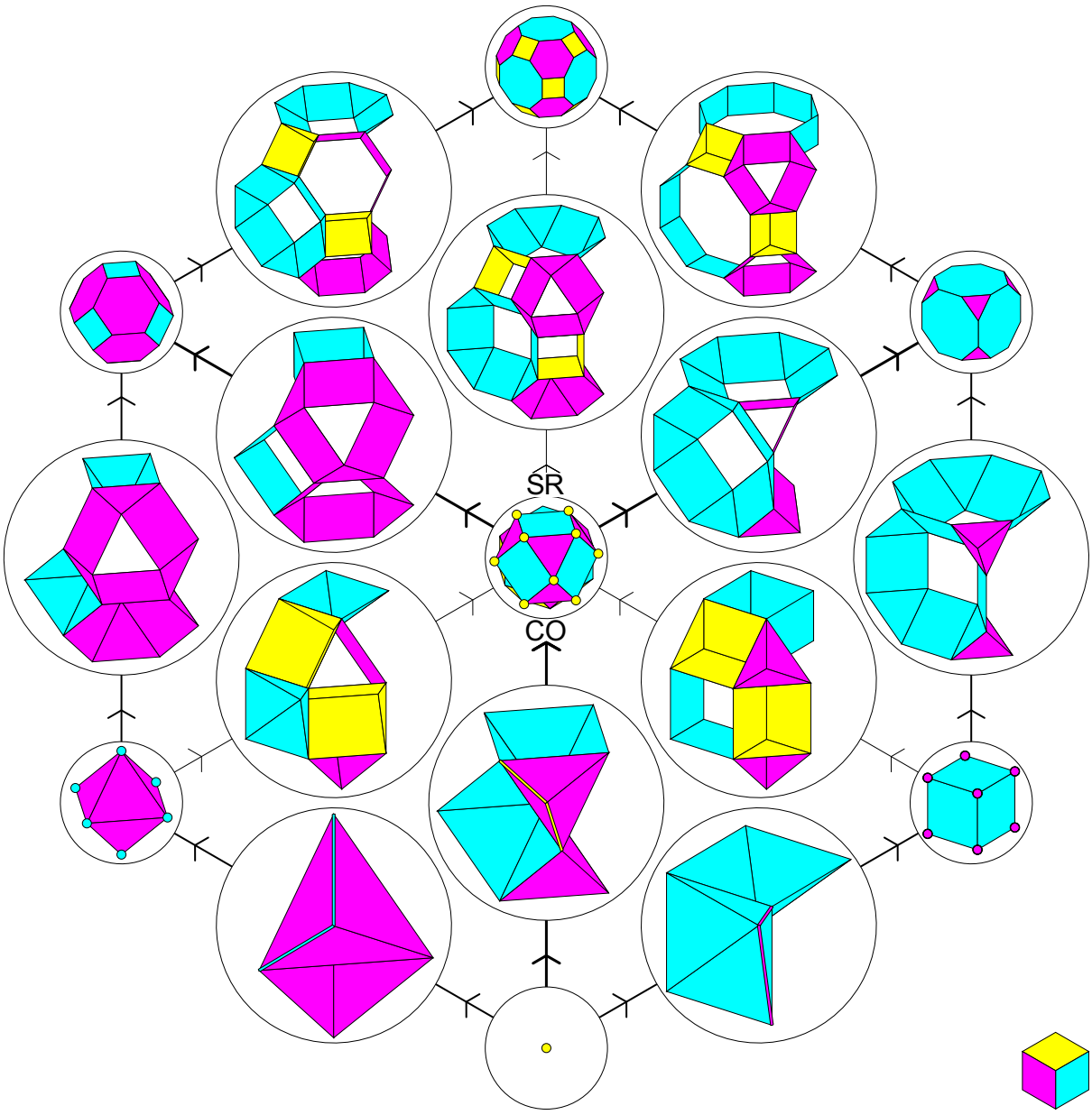

Figure 13B. Partial formation of the Class II horizontal 'front' view 2.5D schema of interlayer components between inner and outer *PP*s. Here, two each of the −ve, ntrl, & +ve elements are shown. In some cases, radial elements are shown as rods; in some other cases, faces of one gender are obscured by faces of another.

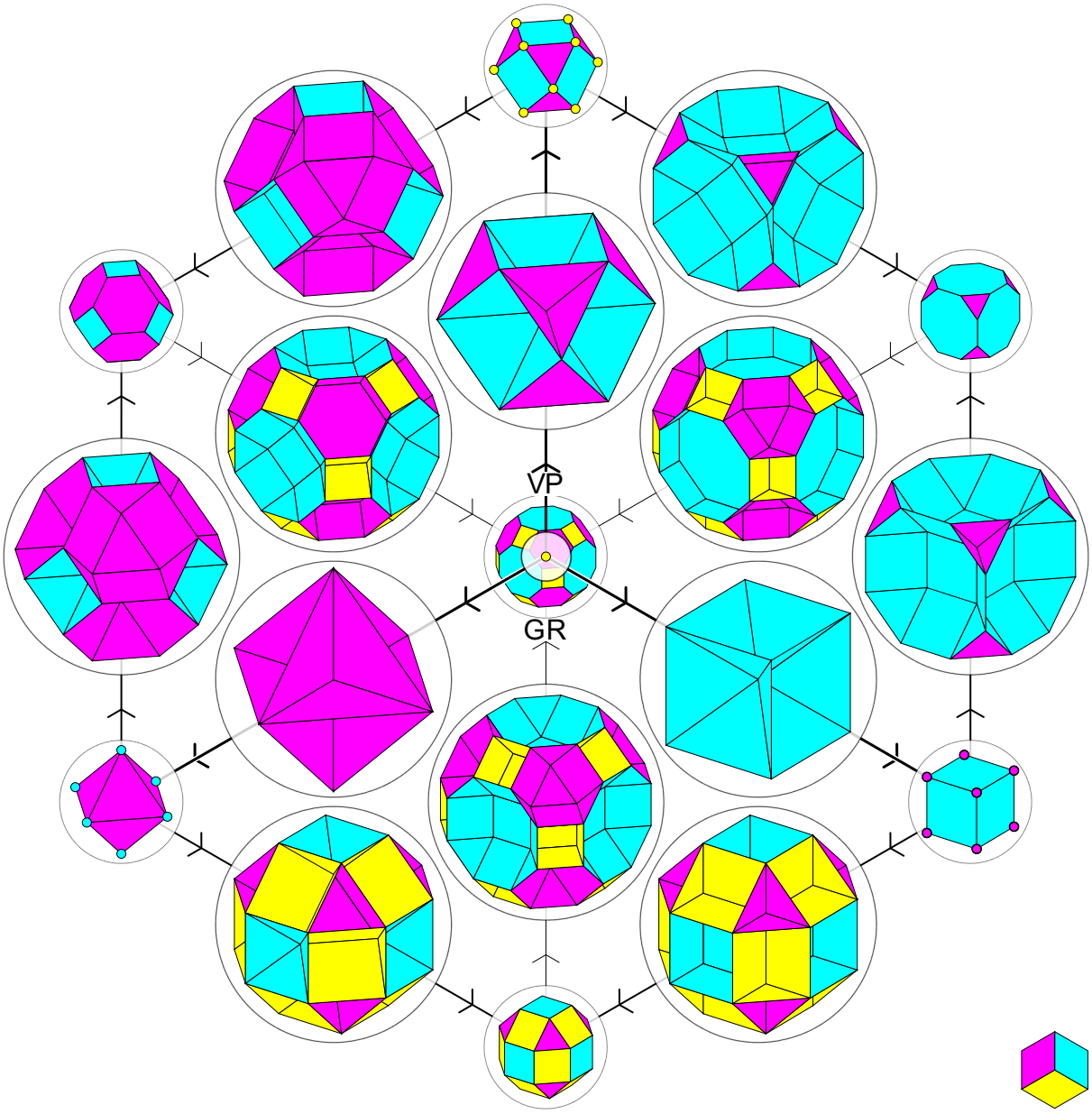

Figure 14. Left: Class II view from below of the cubic schema of interlayer PTs between PPs, with VP (nearest) & GR (furthest) at center; cube seems inverted. Outward radial transformations start from VP; inward radial transformations culminate in GR. All interlayer PTs are radial, coaxial PRS, PYR, or TFM, fill the interlayer space; again, note the overall 2- & 3-fold complementary symmetry.

Figures 14 and 15 show the view from below, with VP (nearest) and GR (furthest) at center, while Fig. 15 shows how the PP s progress through the various strands of development of the relevant transformation/ triangular helix (see Fig. 5).

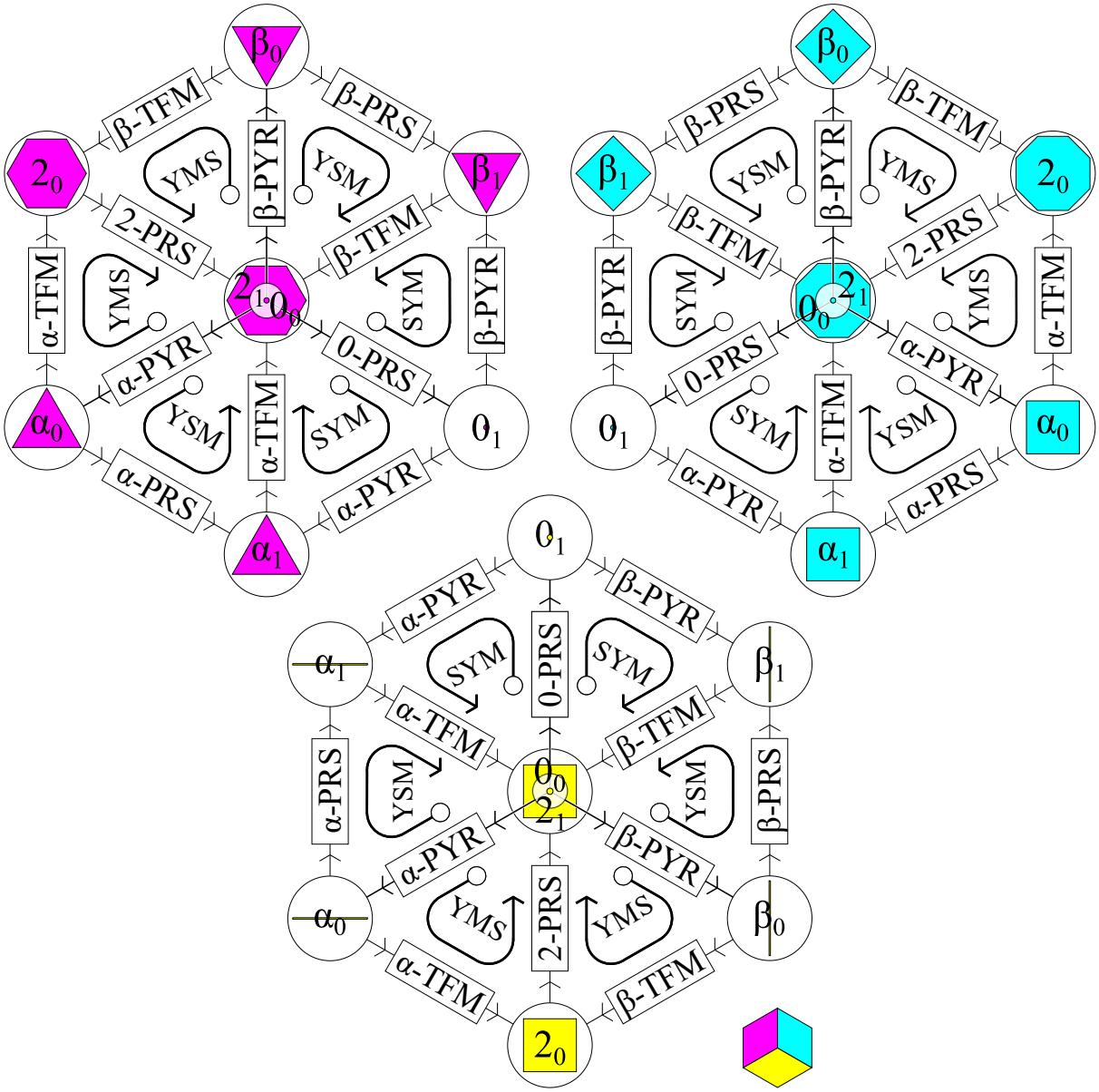

Figure 15. Right: Class II view from below of the triangular helices of sequence of faces of *PP*s and interlayer spatial cells in the cubic schema for +ve (left), ntrl (center), and −ve (right) faces with α|β symmetry about −120°, 0° vertical, and +120° axes, respectively. Helices start with *PRS* (*S*) or *PYR* (*Y*), end with *S* or *TFM* (*M*), with $S{:}\,Y{:}\,M$, $Y{:}\,S{:}\,M$, & $Y{:}\,M{:}\,S$ patterns in equal proportions.

Both Figs. 14 and 15 integrate the 0, α | β, and 2 rhombic schema of faces that I have described in the companion paper to this in this journal issue [4], which work preceded this, and elsewhere [11, 12] (Fig. 1). Faces evolve as the *PP*s progress in the cubic schema, from those of *VP* to those of *GR* (see also Figs. 3 & 4).

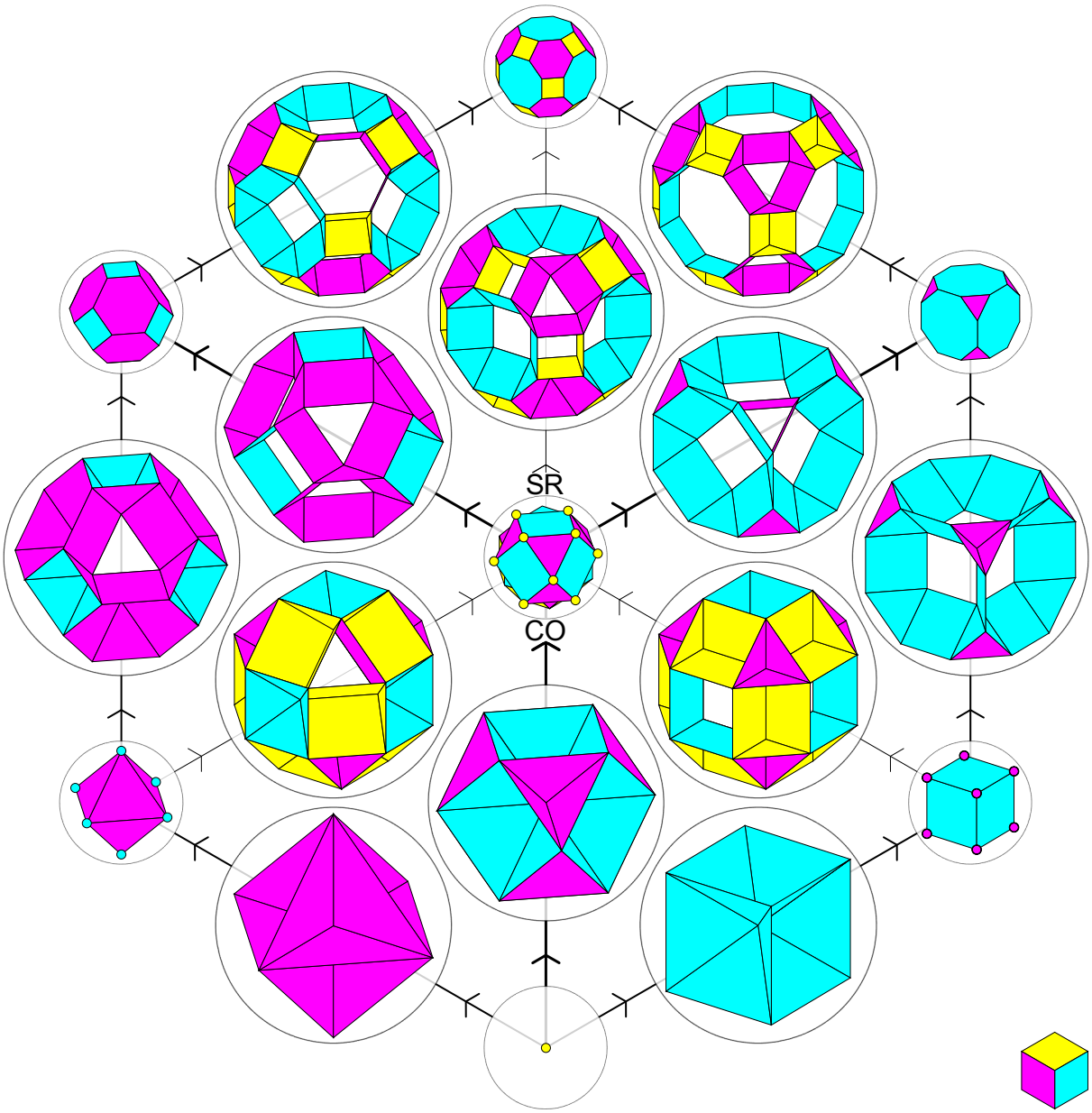

Figure 16. Class II horizontal 'front' view of cubic schema of interlayer components between core and shell, without inner core PP, with CO (nearest) and SR (furthest) at center. These might be treated as *linee occulte*, and used to configure molecular engineering, nanostructure architecture, or dynamic structure for architecture, space structures, deployable structures etc.

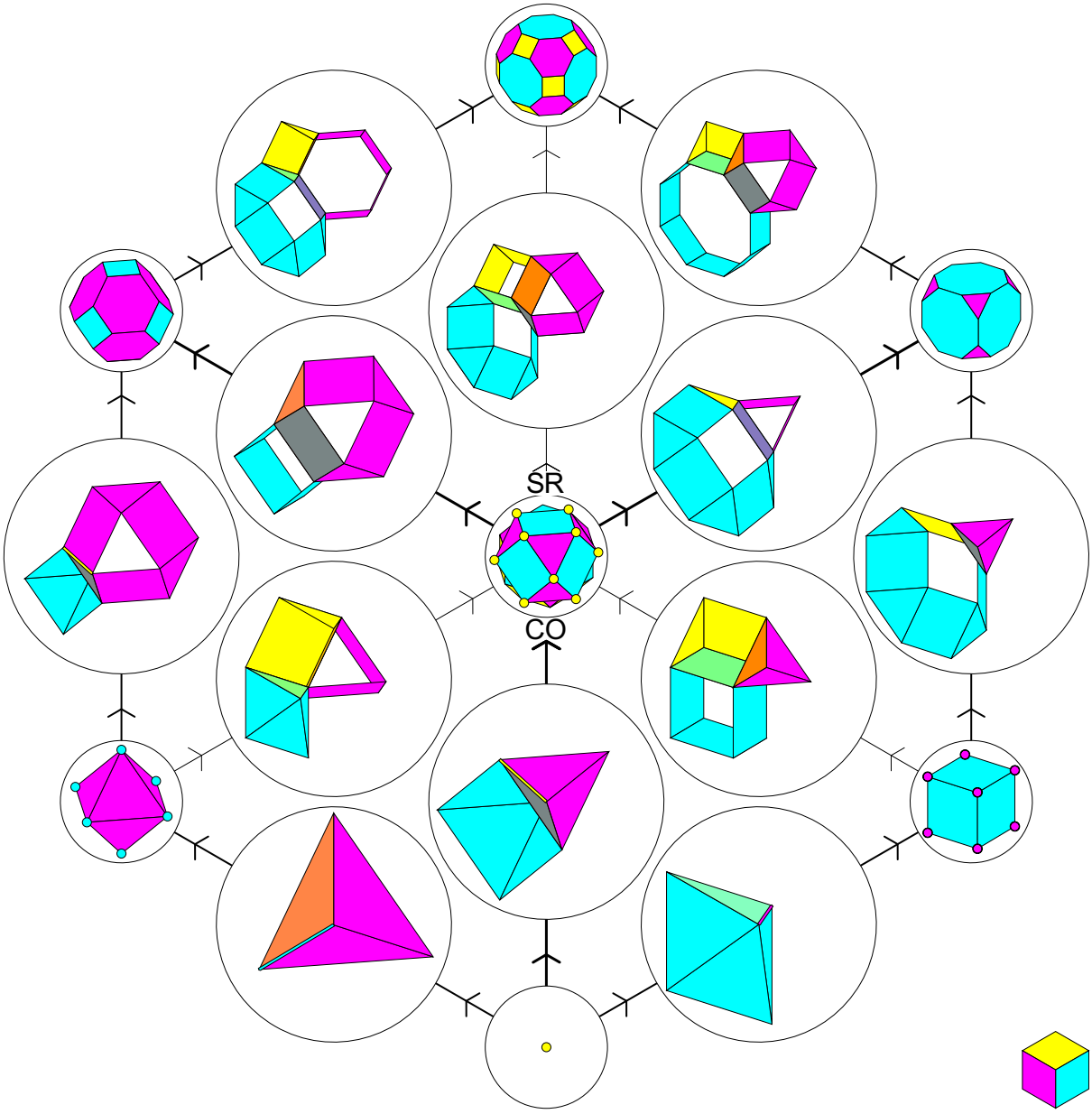

Figure 17: Class II front view with triplet of interlayer components, one of each gender, of cyan, magenta, yellow. Radial *PRS* s are shown as spikes of gender color. Obscured faces shown as overlay of corresponding two colors of 50 % opacity: magenta over yellow shows as orange, yellow over cyan as green, magenta over cyan as dark grey. Within each triplet, web lengths are constant.

4. CONCLUSION

In this paper, I develop the 2.5D cubic schema of polyhedra and the rhombic schema of faces that I have previously advanced to recognize potential core–shell and core–multi-shell configurations of potential relevance to nanoarchitecture, whereby the choice of consecutive PPs delineating the order is constrained by the separation of faces to be PPs that share an edge of the 2.5D cubic schema. These are located concentrically, with coaxial symmetry axes and common edge length. The interlayer space is then regularly divided into all-space filling radial prisms, pyramids, and truncated pyramidal frusta (cupolae), which are described for Class II of {2,3,4} symmetry. The inradii of the PPs show constant increases according to schema axis, which greatly facilitate geometric analysis and composition. The principles apply also to Class I of {2,3,3} and Class III of {2,3,5} symmetry of the polyhedra; it is anticipated to extend the treatment to include Classes IV and V of the polygonal tessellations. Core–multi-shell configurations are also developed, the core–shell configurations being simply subsets of these. The regularity and harmonic order of these configurations is guaranteed by, and further validates the cubic schema of polyhedra, and the rhombic schema of faces previously advanced. These are based on the order of space that I have evolved as an experimental geometer, whereby only certain elements of the polyhedra are regarded as principial, being those that are normal to the symmetry axes. Principial faces may meaningfully consist of 0D vertices or 1D edges, as well as 2D polygons. The order recognizes a key virtual 0D Verticial Polytope (VP) as one of the eight Primary Polyhedra (PPs) of each class. The separation of faces seems key to understanding the morphology, and in a sense, cosmogony, of the polyhedra. These various core–shell and core–multi-shell configurations and their harmonic interrelationship might find use as *linee occulte* in composing various spatial configurations and their dynamic transformations in a variety of fields, which include molecular engineering, nanoarchitecture, biochemistry, biomedical scaffolds, metamaterials, deployable space structures, and in gaining a deeper appreciation of the extraordinary harmonic potential of empirical space.

***

Nomenclature: *, colored ● Class I 3D: OH^* = tetra-tetrahedron ($TR{:}\,TR$); $CO^* = SR\ TR{:}\,TR$; $TO^* = GR\ TR{:}\,TR$ ● Class II 3D: OH, octahedron; CO, cuboctahedron; CB, cube; TO, truncated octahedron; $SRCO$, small rhombic cuboctahedron; TC, truncated cube; $GRCO$, great rhombic cuboctahedron ● Class III 2D: DG, decagon (10-gon); PN, pentagon; RP, rotated pentagon ○ Class III 3D: DC, dodecahedron; $GIRD$, great rhombic icosidodecahedron; IC, icosahedron; ID, icosidodecahedron; $SRID$, small rhombic icosidodecahedron; TD, truncated (trunc.) dodecahedron; TI, trunc. icosahedron ● Class IV 2D: Component arrays: vt, verticial; tr, triangular; hx, hexagonal; rt, rotated (trunc.) triangular; rx, rotated (trunc.) hexagonal; $2t$, 2f triangular (hexagonal); $2x$, 2f hexagonal (dodecagonal) ○ Combined arrays (+ve:−ve): $vt{:}\,vt$, verticial:verticial; $tr{:}\,vt$, triangular:verticial; $vt{:}\,hx$, verticial:hexagonal; $rt{:}\,rx$, rotated (trunc.) triangular:rotated hexagonal; $2t{:}\,rx$, hexagonal (2f triangular):rotated (trunc.) hexagonal; $rt{:}\,2x$, rotated (trunc.) triangular:2f hexagonal (dodecagonal); $tr{:}\,hx = SR\ tr{:}\,hx$, triangular:hexagonal; $2t{:}\,2x$, 2f triangular:2f hexagonal (hexagonal: dodecagonal) ● Class V 2D Component arrays: vt, verticial; sq, square; ns, neutral square; rs, rotated (trunc.) square; $2s$, 2f square (octagonal). ○ Combined arrays (+ve:−ve): $vt{:}\,vt$, verticial:verticial; $sq{:}\,vt$, square:verticial; $vt{:}\,sq$, verticial:square; $rs{:}\,rs$, rotated (trunc.) square:rotated (trunc.) square; $2s{:}\,rs$, octagonal (2f square):rotated (trunc.) square; $rs{:}\,2s$, rotated (trunc.) square:2f square (octagonal); $sq{:}\,sq = SR\ sq{:}\,sq$, square:square; $2s{:}\,2s = GR\ sq{:}\,sq$, 2f square:2f square = $OG{:}\,OG$ ● Generic: −ve, negative; ntrl, neutral; +ve, positive; V, VT, vertex; VP, verticial polytope; NV, neutral vertex; E, EG, edge; NE, neutral edge; F, face; PG, polygon; PT, polytope; NS, neutral square; PRS, prism; PYR, pyramid; SoF, separation of faces; TFM, truncated pyramidal frustum (cupola) ■

Robert C. Meurant □ B.Arch (Hons) (1978) and PhD in Architecture (1984), Univ. of Auckland, New Zealand □ MA Appl. Ling. (2007), Univ. of New England □ Director Emeritus, Institute of Traditional Studies □ University teaching NZ, the U.S., Korea □ Published 6 books, 70 papers, presented papers in New Zealand, the U.S., the U.K., Japan, and Korea □ A director of the Science & Engineering Research Support Society (SERSC) Korea □ Research interests: sacred and traditional geometry, art, and architecture; the polyhedra; the traditional philosophy of art; number, form; structural morphology/geometry; deployable space structures in Space; nanoarchitecture ■

5. REFERENCES

1. K. Critchlow, Order in Space. Thames and Hudson, London, 1969.
2. B. Grünbaum and G. C. Shephard, Tilings and Patterns. W. H. Freeman, New York, 1987.
3. R. C. Meurant, A New Order in Space – Aspects of a Three-fold Ordering of the Fundamental Symmetries of Empirical Space, as evidenced in the Platonic and Archimedean Polyhedra – Together with a Two-fold Extension of the Order to include the Regular and Semi-regular Tilings of the Planar Surface. Int. J. of Space Structures, Vol.6 No.1, Univ. of Surrey, Essex, 1991, 11–32. PDF 06 downloadable at: http://www.rmeurant.com/its/papers/polygon-1.html
4. R. C. Meurant, The morphology of the regular & semi-regular polyhedra and tessellations according to the separation of facial polytopes. European Journal of Applied Sciences, 11(1), 2023, 147–167. PDF 69.
5. R. C. Meurant, Towards a New Order of the Polyhedral Honeycombs: Part II: Who Dances with Whom? Information 2015: L. Li and T.-W. Kuo (eds.), Proceedings of The Seventh International Conference on Information, Taipei, Nov. 25–28, 2015, 369–373. PDF 61.
6. R. C. Meurant, Towards a Meta-Order of the All-Space-Filling Polyhedral Honeycombs through the Mating of Primary Polyhedra. Information, Vol.19, No. 6(B), June 2016, 2111–2124. PDF 62.
7. R. C. Meurant, Sequences of the All Space-filling Periodic Polyhedral Honeycombs. Information 2017. L. Li et al. (eds.), Proceedings of The Eighth International Conference on Information, Tokyo, May 17–18, 2017, 151–154. PDF 63.
8. R. C. Meurant, Expansion Sequences and their Clusters of the All Space-filling Periodic Polyhedral Honeycombs. Information, Vol.20, No.10(A), Oct. 2017, 7345–7362. PDF 64.
9. R. C. Meurant, Form and Counterform in the Periodic Polyhedral Honeycombs. Information 2018: L. Li et al. (eds.), Proc. of The 9th Int. Conf. on Information, Tokyo, Dec. 7–9, 2018, 51–56. PDF 65.
10. R. C. Meurant, Towards a New Order of the Polyhedral Honeycombs: Part III: The Developed Metaorder, Form and Counterform. Information, Vol.22, No.1, Jan. 2019, 23–45. PDF 66.
11. R. C. Meurant, A New 2.5D Schema of the Regular & Semi-regular Polyhedra and Tilings: Classes II and IV. Information, L. Li, R. Ashino, & C.-C. Hung (eds.), Proceedings of The Tenth International Conference on Information, Tokyo/Zoom, Mar. 6–7, 2021, 29–34. PDF 67.
12. R. C. Meurant, A Novel 2.5D Schema of the Regular and Semi-regular Polytopes and their Sequences, with Analysis by Polytope and Surface Elements. Information Journal, International Information Institute, Vol.24, No.2, June 2021, pp.51–64. PDF 68.
13. R. C. Meurant, The Aesthetics of the Sacred: A Harmonic Geometry of Consciousness and Philosophy of Sacred Architecture (3rd ed.), The Opoutere Press 1989 ISBN 0-908809-02-6. (PhD thesis, Univ. of Auckland, 1984). Available from the author, see http://www.rmeurant.com/its/books.html
14. R. C. Meurant, The Myth of Perfection of the Platonic Solids. People and Physical Environment Research PAPER Conference on Myth Architecture History Writing, Univ. of Auckland 1991. PDF 07.

Supplementary Information: References [3−12, 14] as PDFs (06, 69, 61−68, 07), and PDF 70 of this paper in color or greyscale, are available at http://www.rmeurant.com/its/papers/polygon-1.html